AXIAL LOAD TRANSFER IN LARGE-SCALE PHYSICAL MODEL DRILLED SHAFT FOUNDATIONS

A Thesis presented to the Faculty of the Graduate School

University of Missouri-Columbia

In Partial Fulfillment of the Requirements for the Degree

Master of Science

---

by
MARTIN L. WALLACE

Dr. J. Erik Loehr, Thesis Supervisor

MAY 2019

The undersigned, appointed by the dean of the Graduate School, have examined the thesis entitled

AXIAL LOAD TRANSFER IN LARGE-SCALE PHYSICAL MODEL DRILLED SHAFT FOUNDATIONS

Presented by Martin L. Wallace,

A candidate for the degree of Master of Science in Civil Engineering

And hereby certify that, in their opinion, is worthy of acceptance.

Professor J. Erik Loehr, P.E.

Professor John J. Bowders, P.E.

Professor Francisco Gomez

ACKNOWLEDGEMENTS

I would like to thank my advisor Dr. J. Erik Loehr for advising me throughout my graduate career. He was an excellent teacher who challenged me to be the best that I could be in the classroom, in the laboratory and ultimately as an engineer. I am forever grateful for the advice, assistance and encouragement he gave me throughout this project and my academic career.

I would also like to acknowledge Dr. John Bowders as a pivotal figure in my early engineering career. I would like to thank him for bringing me on as an undergraduate research assistant in the Spring of 2016 and encouraging me to continue my education and pursue a graduate degree. I have grown immeasurably from the time we first met to today. Thank you for being gracious with your time and knowledge.

I also greatly appreciate Dr. Francisco Gomez for taking time out of his busy schedule to sit on my thesis committee. I greatly appreciate his comments that helped make this thesis the best it could be.

Creation and execution of this testing program would not have been possible without the support of Andrew Boeckmann. I cannot thank him enough for spending countless hours in the laboratory guiding me toward the ultimate end goal. Thank you for all your help and advice on my academic and professional career.

This work would not have been possible without the work from countless colleagues. Special thanks to my fellow graduate students and friends, Zakaria El-Tayesh and Elgin Burton for their help on this project. Special acknowledgement to Isaiah Vaught who helped me from the start of the testing program to the end. His problem-solving skills and hard work helped keep

this project moving forward. This work would not have been possible without the help from numerous undergraduate researchers. Thanks to Stacey Bonderer, Dustin Freeman, Jon Knight and Sam Runge for their unwavering commitment to this project.

Thanks to Aaron Saucier for his help in the laboratory and efforts coordinating work out at the RTF. Thanks to Michael Carhar for his expertise in creating and troubleshooting our data acquisition system. Special thanks to Rex Gish, Ghassan Al Bahhash and Matthew Marciniak from Engineering Technical Services for their help throughout the project.

Funding for this project was provided by the California Department of Transportation.

TABLE OF CONTENTS

LIST OF FIGURES

LIST OF TABLES

AXIAL LOAD TRANSFER IN LARGE-SCALE PHYSICAL MODEL DRILLED SHAFT FOUNDATIONS

Martin L. Wallace, Masters Candidate in Civil Engineering

Dr. J. Erik Loehr, Thesis Supervisor

ABSTRACT

Drilled shaft foundations are a widely implemented type of deep foundation used to support heavy loads from superstructures such as buildings and bridges. Uncertainties exist in the axial load transfer behavior of drilled shafts subject to loading and unloading cycles. A better understanding of the changes in soil reload stiffness can lead to a better understanding of the load deformation response. A study was undertaken using a 16-inch diameter by 28-inch tall physical model drilled shaft foundation. A total of nine static load tests were performed in a five-foot diameter by five-foot deep calibration chamber where soil conditions could be controlled. Soils tested were a loose clean sand, dense clean sand and compacted silty sand. A bladder system was used to apply vertical effective stress to the soil to simulate depths of embedment up to 70 feet below the ground surface. Based on test results, a relationship between the reload stiffness and displacement was developed. The relationship indicates that the reload soil stiffness is initially large before decreasing to a constant value as displacement increases depending on soil configuration. Results from three different soil configurations were normalized based on the constant behavior observed at large displacements. A relationship between the normalized reload stiffness versus displacement was created. This relationship can be used to predict the reload stiffness for model drilled shaft foundations in coarse grained soils.

Chapter 1 Introduction

1.1 Objective and Methodology

The objective of the work presented in this thesis is to examine the base response of drilled shaft foundations in coarse grained soils after axial loading and subsequent unloading and reloading. Limitations exist pertaining to the full mobilization of tip resistance in drilled shaft foundations. A better understanding of the soil stiffness response can lead to more reliable and economical drilled shaft design.

The methodology used to achieve these objectives was to conduct laboratory axial load tests on model drilled shaft foundations. Load tests were performed on small scale models constructed to replicate the base (tip) of a full-size drilled shaft foundation. The model foundations were 16 inches in diameter by 30 inches tall and constructed to mimic the design and behavior of a typical drilled shaft foundation. A 5-foot deep by 5-foot diameter calibration chamber was used to replicate field conditions during testing. In this apparatus, soil conditions can be controlled to reduce variability. A casing was used in some tests to eliminate side resistance and isolate behavior at the base of the foundation. In other tests a casing was not used. The setup of the experimental apparatus is similar to conventional field load tests. Soil can be placed in a uniform manner depending on a target density and a bladder system can be used to apply vertical effective stress. The versatility of the experimental apparatus allows for investigation of axial load-settlement behavior at a variety of vertical effective stresses. In this setup, the calibration chamber is capable of applying vertical effective stress as high as 7200 psf simulating depths in the range of 60 to 70 feet below the ground surface.

A total of nine tests were performed in the experimental apparatus. The load test procedure performed is similar to ASTM D1143 Static Load Test for Deep Foundations under Compressive Load. The tests were divided into two groups depending on if a casing was used during testing or not. The tests are also divided based on the soil type and target density. Each load test was instrumented to measure axial load, displacement, vertical effective stress and soil density. The data were analyzed and a relationship between the reload soil stiffness and displacement was developed. Results of all test and analyses are presented in this thesis.

1.2 Organization of Thesis

This thesis is organized into six chapters. In Chapter 2 a review of relevant literature is presented. General information on drilled shaft foundations is described. Relevant literature on load transfer in drilled shafts in coarse grained soils is discussed. The importance and procedure for performing a static load test on a pile foundation as outlined by the American Society of Testing and Materials (ASTM) is included in this chapter.

A description of the experimental apparatus used to complete the work is described in Chapter 3. In chapter 3 the apparatus assembly is presented including the chamber, top and bottom plate and the reaction frame. Relevant equipment such as the hydraulic jack and hydraulic pump used to apply load during the load test are detailed including relevant calibrations. Instrumentation used during testing such as a load cell, pressure transducers, linear variable differential transformers (LVDTs) and soil density are explained. Characteristics of the soil used in the work in addition to the tests performed to quantify their properties are included. A detailed step-by-step testing procedure is also detailed in Chapter 3.

Results from the testing program are presented in Chapter 4. Chapter 4 details each of the nine tests performed across two different soil types. The tests are also divided between tests that included a casing and those that did not. Testing conditions including soil density, water content and average applied vertical effective stress are detailed. Any problems or relevant observations encountered during testing are described on a test by test basis.

In Chapter 5 data analysis procedures and results are presented. The methods used to characterize the reload soil stiffness during axial load tests are detailed. A relationship between soil stiffness and displacement is created. Finally, Chapter 6 presents a summary of the thesis, a detailed set of conclusions based on analysis of the results and recommendations for future work.

Chapter 2 Literature Review

In this chapter, drilled shaft foundations are defined and axial load transfer in drilled shaft foundations is discussed. The standard procedure for performing a static axial load tests based on ASTM standards is described.

2.1 Drilled Shaft Foundations

Drilled shafts are a type of deep foundation. Deep foundations are long, slender structural members that penetrate deep into the ground (Coduto et al., 2016). Geotechnical engineers and contractors could also refer to a drilled shaft as a pier, drilled pier, bored pile, cast-in-place pile, caisson, drilled caisson or cast-in-drilled-hole (CIDH) pile. Drilled shafts are used widely in supporting large loads from super structures such as buildings, bridges and signage due to their minimally intrusive nature (Thiyyakkandi et al., 2014).

The construction process consists of drilling a cylindrical hole in the ground, placing a prefabricated steel reinforcing cage into the hole, then filling with concrete (Coduto et al., 2016). Drilled shafts are non-displacement piles and differ from other types of pile foundations in that the soil is excavated with a drilling rig and auger before construction of the foundation begins. Drilled shafts typically range from 3 to 5 feet in diameter and 20 to 80 feet in length but can be as large as 10 feet or more in diameter and extend up to 200 feet below the ground surface (Coduto et al., 2016). Selection of a drilled shaft foundation hinges on multiple factors including the anticipated use, structural loads, cost of construction and soil conditions. Typically, drilled shaft foundations have lower equipment mobilization costs and simpler construction processes compared to other deep foundations such as driven piles. The construction process allows for soil conditions to be confirmed as installation occurs. Construction can occur in a variety of soil

conditions including soils with large cobbles or boulders. The foundation type can also be founded in many different types of bedrock.

Drilled shafts can be loaded in axial compression, axial tension and laterally. Figure 2.1 shows how loads can be applied to a drilled shaft. Axial loads are applied parallel to the longitudinal axis and lateral loads are applied perpendicular to the longitudinal axis. A drilled shaft foundation transfers loads to the soil through a combination of side resistance and tip resistance. Tip resistance can also be referred to as the toe bearing resistance, point bearing resistance or end bearing resistance (Coduto et al., 2016). Tip resistance is the interaction between the area of the base of the foundation and the underlying soil. Side resistance, which can also be referred to as skin friction, is the resistance developed in the interface between the soil and concrete along the length of the foundation (Coduto et al., 2016).

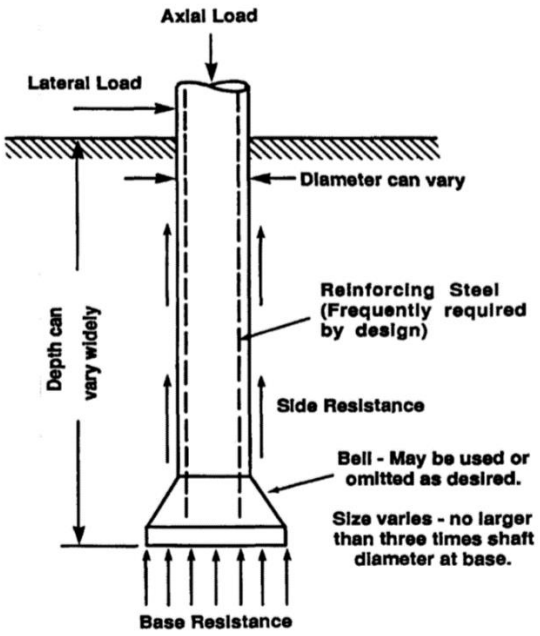

Figure 2.1 Schematic of drilled shaft with different load combinations from Reese and O'Niell (1999).

2.2 Load Deformation Response in Coarse Grained Soils

Drilled shaft foundations support axial loads with a combination of side and base resistance. Extensive field testing throughout the world has proven that a substantial portion of the applied axial load is carried in side resistance (Reese and O'Niell, 1999). Extensive field loading tests of drilled shaft foundations presented or documented by Reese and O'Niell (1988) and Chen and Kulhawy (1994) show the initial compressive load increments are carried in side resistance. Side resistance can be fully mobilized at relatively small downward displacements. Mobilization of tip resistance only occurs after the foundation undergone some displacement, typically ½ inch or more (Reese and O'Niell, 1999). Tip resistance is largely dependent on the degree of shaft displacement. Figure 2.2 shows a relationship between displacement and tip resistance developed by Reese and O'Niell, 1999. In this figure, tip resistance as a percentage of the ultimate base resistance increases with shaft displacement as a percentage of base area. Tip resistance likely comprises a large portion of the total resistance at the ultimate limit state (Reese and O'Niell, 1999).

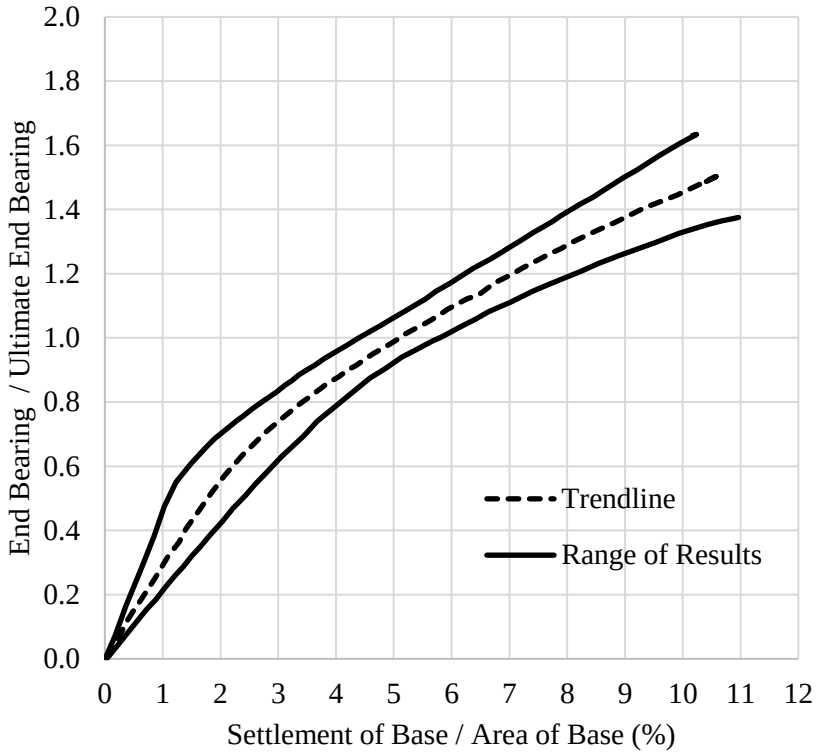

Figure 2.2 Normalized base load transfer for drilled shaft in cohesionless soil from Reese and O'Niell (1999)

Modeling the deformation response of drilled shafts under axial load has proven to be especially difficult and even advanced numerical methods are not applicable to routine calculations (Dias and Bezuijen, 2017). It is challenging to model the variety of physical processes involved in construction of drilled shaft foundations and accurately predict their load-settlement behavior. Due to difficulties modeling load-settlement behavior, load transfer models have relied heavily on more objective or empirical approaches. One of the first load transfer methods was developed by Coyle and Reese (1966). The method iteratively calculates pile load from an inputted toe displacement. The method divides the pile into discrete lengths and uses mobilization functions to predict pile load. Unfortunately, the method is only able to examine pile loading and cannot examine a non-elastic pile loading cycle where loading, unloading and

reloading occur. An example of a load test with loading, unloading and reloading is shown in Figure 2.3. The load transfer method developed by Coyle and Reese (1966) cannot model irreversible deformations and residual loads that have been observed in field load tests (Dias and Bezuijen, 2017).

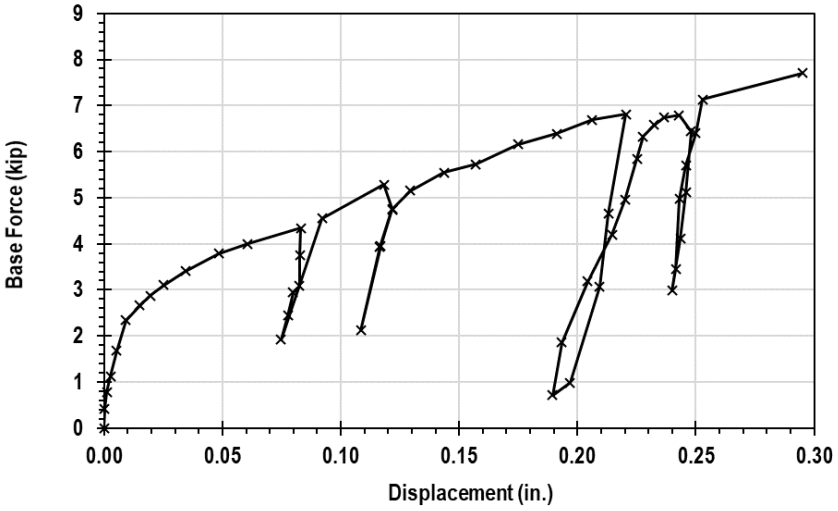

Figure 2.3 Example of a typical load test with loading and unloading cycles and permanent deformations from Gavin and Lehane (2007)

Dias and Bzeuijen, 2017 proposed a modified version of the load-transfer method, which includes unloading paths and can be defined at any level along the pile. The model uses Coyle and Reese (1966) as a backbone to determine tip resistance mobilization. Figure 2.4 shows how the model defines non elastic deformation as a result of loading, unloading and reloading on a plot of tip resistance versus displacement. For loading, the model requires an ultimate base resistance ($q_{b\text{-}max}$) to be defined at a relative displacement ($\Delta\delta^{T}$) at the tip. The ultimate base resistance ($q_{b\text{-}max}$) represents full mobilization of the tip resistance. A rebound factor (Rb) is used to model the variable slope of soil stiffness during unloading and reloading. The rebound factor defines the relative displacement necessary to reach a state of zero toe reaction. The rebound

factor is a function of the total mobilized base resistance ($q_{b\text{-}max}$). A lower base resistance relative to the ultimate base resistance will equate to a smaller rebound factor. The slope of the unload or reload soil stiffness will change depending on the relative degree of tip resistance mobilization.

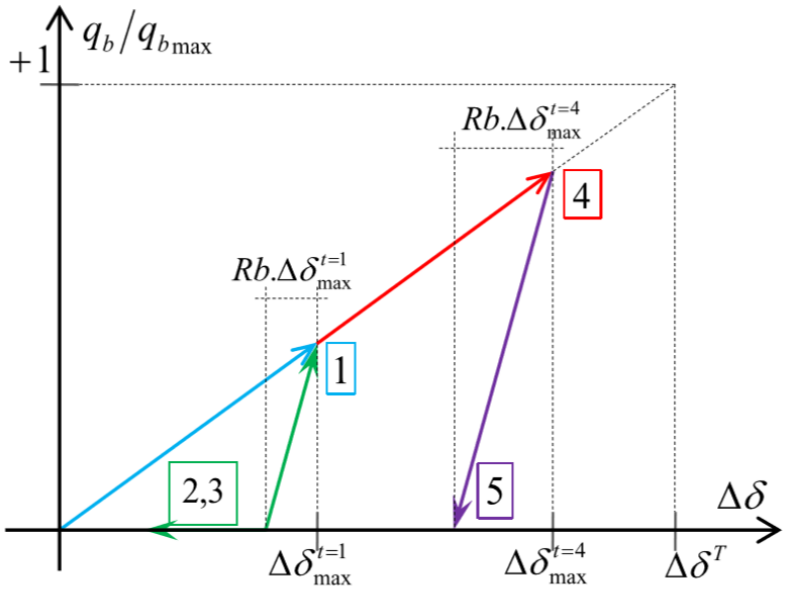

Figure 2.4 Tip resistance (q_b) mobilization model from Dias and Bezuijen (2017)

The model proposed by Dias and Bezuijen (2017) only applies for load transfer in piles where positive displacement occurs. Negative displacement would mean the pile tip is not in contact with the soil. Figure 2.5 shows an equation defining the linearity of the reload and unload stiffness portion of the curve proposed by Dias and Bezuijen (2017). The equation defines linearity of the soil stiffness under reload or unload by an exponential function using λ as a toe mobilization function, relative tip mobilization ($q_b/q_{b\text{-}max}$) and the relative displacement ($\Delta\delta/\Delta\delta^T$).

$$\frac{q_b}{q_{b-\max}} = \left(\frac{\Delta\delta}{\Delta\delta^T}\right)^{\lambda}$$

Figure 2.5 Equation defining the linearity as an exponential function in the model proposed by Dias and Bezuijen (2017)

The parameter of the exponential toe mobilization model (λ) defines the linearity of the reload or unload stiffness depending on the degree of tip resistance mobilization and percentage of total displacement. Figure 2.6 shows different values for the toe mobilization parameter as degree of mobilization and percentage of displacement changes. In order to calibrate the model from Dias and Bezuijen (2017) axial load tests on full size drilled shafts in the field is required.

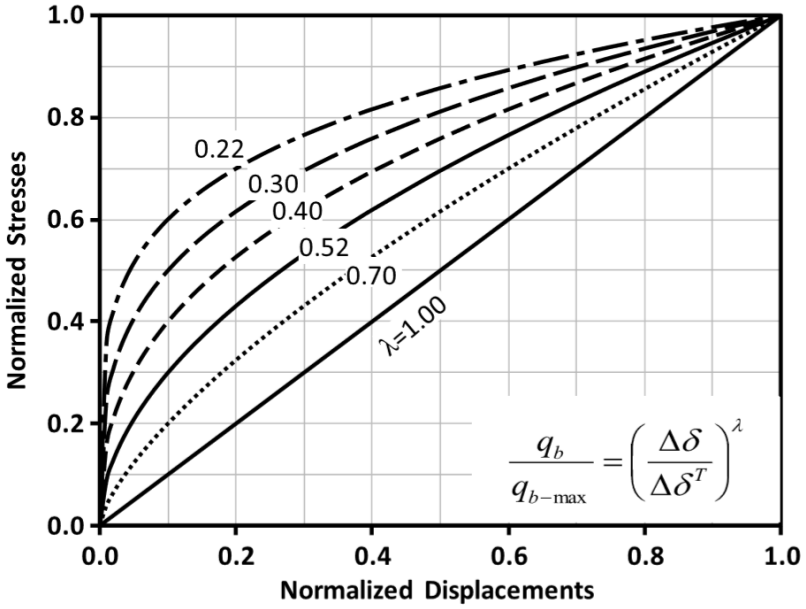

Figure 2.6 Normalized stresses (q_b / $q_{b\text{-}max}$) versus normalized displacements ($\Delta\delta/\Delta\delta^T$) for different values of the toe mobilization parameter (Dias and Bezuijen, 2017).

Gavin and Lehane (2007) performed axial load tests on a variety of deep foundation types including drilled shafts, open ended pipe piles and closed ended pipe piles. The results of the load test on a model drilled shaft foundation were shown in Figure 2.3. The goal of their research was to examine the effect of soil prestress on the load-settlement behavior. Multiple load tests

were performed to evaluate the load-settlement behavior. The results of the tests show that the load-settlement response is essentially linear up to a strain level that is controlled by the stress history of the sand at the pile base (Gavin and Lehane, 2007). The degree of prestress in the soil below the tip of the model drilled shaft correlates to the point of significant degradation of the base stiffness. The point where the base stiffness began to degrade occurred at higher strains in sands that had been prestressed to larger values. The effect of prestress was examined in tests with a model drilled shaft, virgin loading and unloading soil stiffness were examined by loading, unloading and reloading the foundation at multiple points throughout the load test. It was evident that prestressing the soil in a static load test had no effect on the degradation of the soil stiffness when comparing the virgin soil stiffness to the virgin reload stiffness. Base stiffness degradation is primarily a function of the prestress in the soil prior to pile installation.

2.3 Base Load Response in Post Grouted Drilled Shaft Foundations

A motivation for examining the load-settlement behavior of model drilled shaft foundations is to provide more insight into the base resistance of post-grouted drilled shafts (PGDS). Post grouting involves pressure injecting a grout mixture consisting of Portland cement and water beneath the tip of the drilled shaft via a grout delivery system after the concrete has cured (Loehr et al., 2017). Post grouting has been used in Asia and Europe to improve pile capacity since the 1960s (Thiyyakkandi et al., 2014). The method has also been reported to stiffen the load-deformation response of a drilled shaft by pre-mobilizing side and tip resistance (Loehr et al., 2017).

In PGDS, it has been reported that the load-displacement response of the shaft is greater than the stiffness of a conventionally constructed shaft in similar materials (Thiyyakkandi et al., 2014). In an examination of the base resistance of grouted and un-grouted drilled shafts a study was undertaken by Thiyyakkandi et al. (2014) to determine the effect of post grouting on base load transfer in cohesionless soils. Axial load tests were performed on model drilled shaft foundations in a calibration chamber. It was found that the reload soil stiffness in an un-grouted drilled shaft was similar to the soil stiffness of a post grouted drilled shaft of the same size. Figure 2.7 shows a conceptual normalized tip resistance versus displacement plot for conventional un-grouted and post grouted drilled shafts. A typical post grouted drilled shaft will follow the path C-B-D compared to a conventional un-grouted shaft which will follow A-B-D. In order to determine the reload stiffness a loading cycle consisting of loading up to the anticipated grout pressure, unloading and reloading was performed on an un-grouted drilled shaft. Preloading the soil from post grouting results in a stiffer axial load-displacement response compared to a conventional un-grouted shaft. The stiffer response of post grouted shafts means the same load will result in significantly smaller displacements compared to conventional un-grouted drilled shafts.

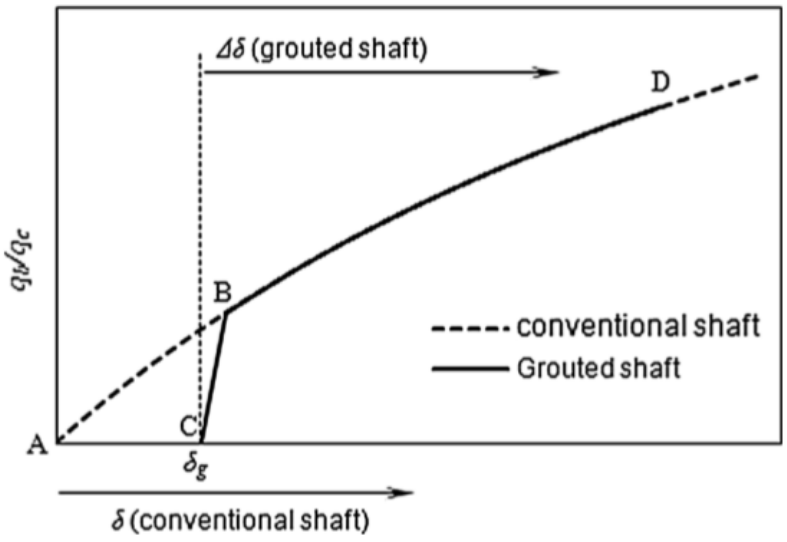

Figure 2.7 Conceptual response of grouted and un-grouted drilled shafts (Thiyyakkandi et al., 2014).

2.4 Static Load Tests

Load tests can provide much more accurate assessments of the axial capacity of drilled shaft foundations compared to empirical or semi-empirical methods (Coduto et al., 2016). Load tests can also be used to determine the axial tensile or lateral capacity of piles. Only axial compression load tests will be discussed in this section. Using axial load-settlement data collected in a load test, the base response of drilled shaft foundations in coarse grained soils can be determined.

A schematic of a typical load test setup as described by ASTM D1143 is shown in Figure 2.8. The standard method for testing piles in axial compression is described in ASTM D1143 Standard Test Method for Pile Under Static Axial Compressive Load. In order to conduct a load test, an apparatus that can apply desired loads to the pile is required. Applying loads to a test pile can be done in several ways but most commonly with a hydraulic jack. Typically, the hydraulic

jack will act against a reaction frame anchored to reaction piles installed on either side of the test pile.

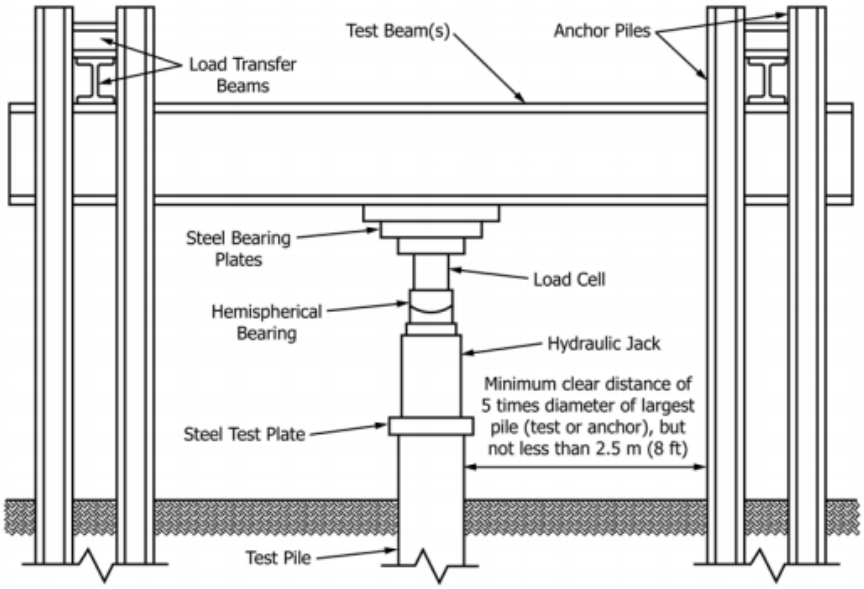

Figure 2.8 Schematic of hydraulic jack acting against anchored reaction frame (ASTM D1143, 2013.)

The most applicable load test method to this thesis is outlined in ASTM D1143, Procedure A: Quick Test. The result of the test produces a load-settlement curve for the test pile. The method involves applying load in increments of 5% of the anticipated failure load. The load is added in a continuous fashion immediately following the completion of movement readings from the previous load step. The load should be added and removed in the same fashion with a constant load held on the test pile for no shorter than 4 minutes and no longer than 15 minutes. Specific details relating to setup of a test pile, instrumentation, safety, measurements, and other requirements can be found in ASTM D1143.

2.5 Summary

In this chapter an overview of drilled shaft foundations including post grouted drilled shafts was given. Post grouting as a solution to some of the shortcomings associated with conventional drilled shaft construction was discussed. Relevant information regarding load transfer and base response of drilled shafts was presented. A procedure for a standard static axial load test as outlined by ASTM was also included in this chapter.

Chapter 3 Experimental Apparatus and Testing Procedure

The experimental apparatus used in this testing program is described in detail in this chapter. The apparatus consists of a chamber where a model drilled shaft foundation and soil are placed, a reaction frame to resist axial load applied by a hydraulic jack, a bladder system to apply the desired overburden stress to the soil and an instrumentation system to record relevant data. In this chapter a testing procedure is outlined.

3.1 Chamber Assembly and Reaction Frame

The chamber assembly consists of a bottom plate, a cylindrical steel chamber, and a top plate. A photo of the chamber assembly and reaction frame is shown in Figure 3.1 The chamber is 5 feet tall by 5 feet in diameter with a ¾ inch wall thickness. The cylindrical steel chamber rests on top of the bottom plate and is attached to the top and bottom plates using ten 1-inch diameter A325 steel bolts. The bottom plate rests on a bottom assembly consisting of two W18x130 steel beams. The top plate is reinforced with two C12x20.7 channel sections. The top plate has a 15-inch square opening centered below the cross brace. During testing, a reaction frame rests on the channel sections. The reaction frame is attached to the W-sections below the bottom plate with eight 1-¼ inch 150 ksi threaded DYWIDAG bars with anchor plates and hand tightened structural steel bolts.

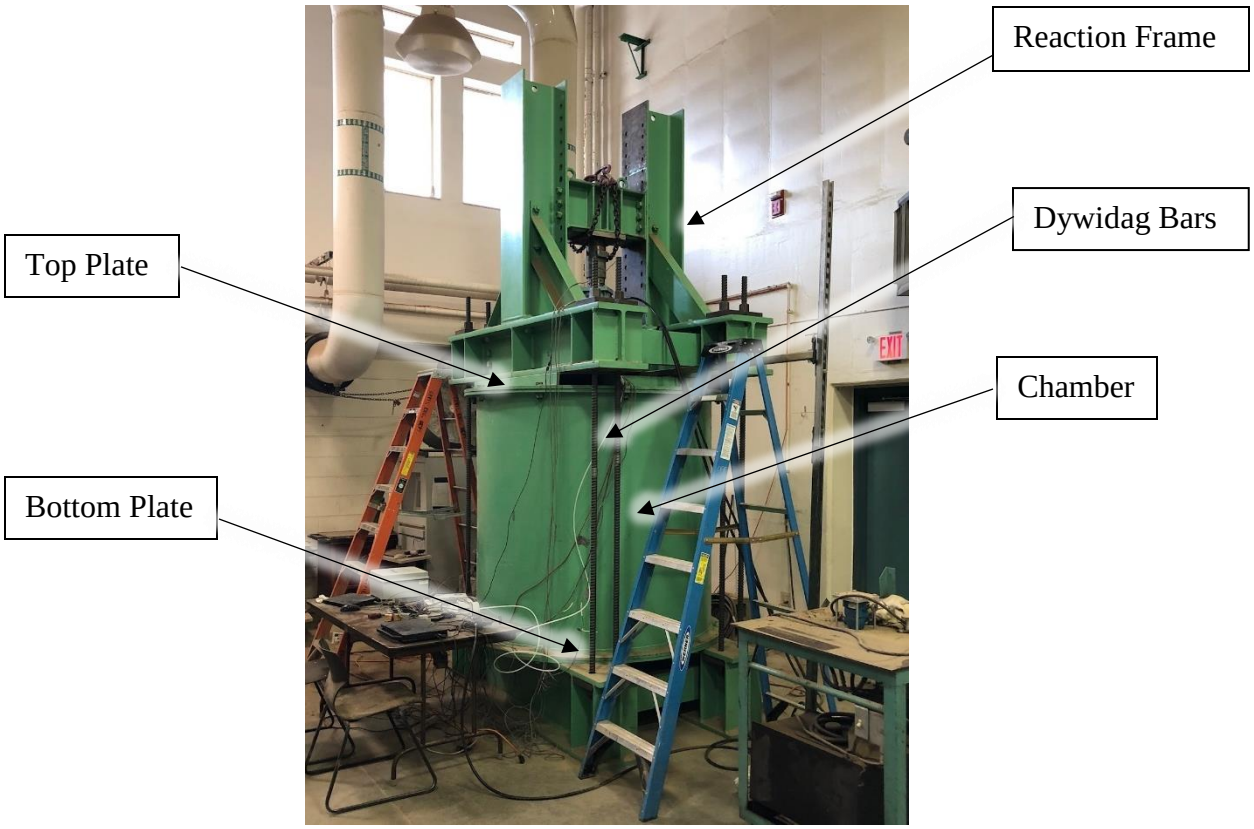

Figure 3.1 Experimental setup showing the reaction frame, dywidag bars, top plate, chamber and bottom plate

A photo of the reaction frame detailing the cross brace, load cell and hydraulic jack is shown in Figure 3.2. The reaction frame consists of two W12x152 steel beams acting as a base and two vertical HP12x74 piles. A cross brace of two back-to-back MC12x45 steel beams connect the vertical HP12x74 piles. The height of the cross brace can be adjusted. A load cell is connected to the cross brace using four threaded bars. The canister type load cell from Lebow Associates, Inc. has a capacity of 150,000 pounds.

A hydraulic jack is connected to the load cell using one threaded bar. Spacers connecting the load cell and hydraulic jack allow the jack to spin for access to hydraulic hose connections. The hydraulic jack has a stroke of approximately 14 inches. A four-way hydraulic control valve and manually operated hydraulic regulator control the pressure supplied to the hydraulic jack.

The hydraulic control valve is held open during testing while the hydraulic regulator is adjusted to the desired pressure. The hydraulic pump has a maximum capacity of 6000 psi.

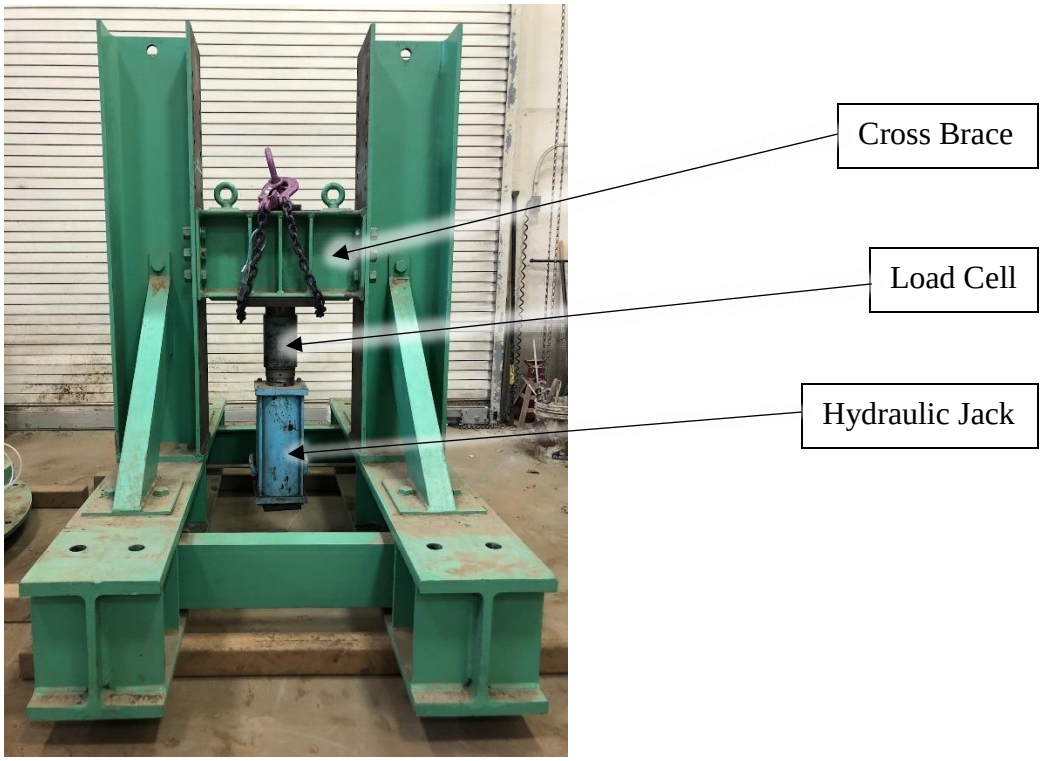

Figure 3.2 Photograph of the reaction frame showing cross brace, load cell and hydraulic jack

A schematic of the experimental apparatus used in this testing is shown in Figure 3.3. The location of the model foundation in the chamber is detailed in the schematic. The figure also shows the location of the soil, bladder system, steel ring and casing during a typical test.

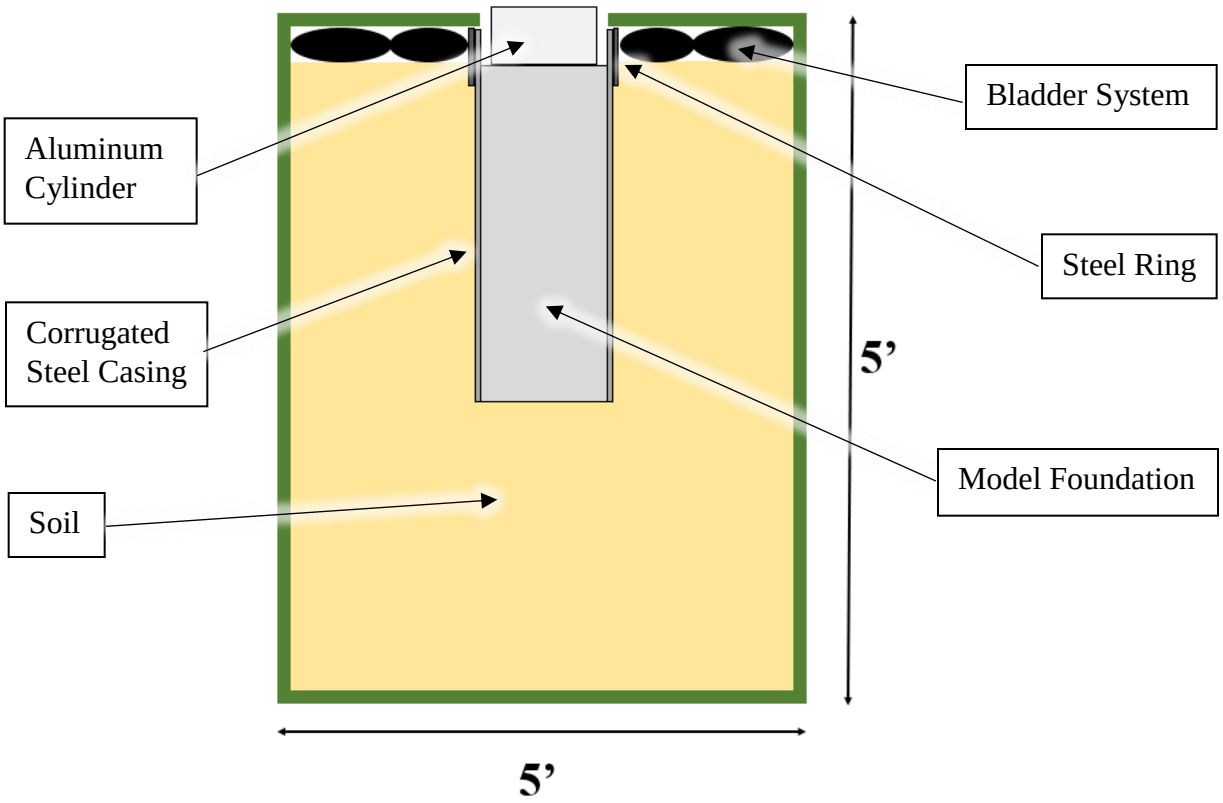

Figure 3.3 Schematic of the experimental apparatus showing the location of the model foundation, soil, bladder system and casing

3.2 Bladder Systems

The experimental apparatus utilizes a bladder system to apply uniform overburden stress to the soil in the chamber. Figure 3.4 shows the location of the bladder system in the chamber assembly during a typical test. The bladder system allows for tests to be performed at various effective depths of embedment up to 70 feet. Two commercially available butyl rubber tire tubes were attached to the building air supply and filled to apply overburden stress to the soil. The inflated tubes apply overburden stress to the top of the soil while reacting against the underside of the top plate and walls of the chamber. The rubber tubes are flexible enough to expand and occupy all available space between the soil surface and the bottom of the top plate. Ensuring all space is occupied by the bladders ensures that uniform vertical stress is applied to the soil. The

bladder system consisted of two concentric rubber tire tubes. The tubes consist of one 11.2/12.4R24 tube and one 16.9/18.4R38 tube. The smaller 11.2/12.4R24 tube fits snug around the outside of a steel ring and corrugated steel casing. The larger 16.9/18.4R38 tube fits to the outside of diameter of the 11.2/12.4R24 tube and expanded to the diameter of the chamber. A large rubber tire width was desired in order to reduce the risk of tube failure by ensuring the tires were never fully inflated.

A six-inch long, 19-inch diameter steel ring was used around the top portion of the corrugated steel casing to support the bladder system during testing. The steel ring contacted the underside of the top plate and enclosed the 15-inch square hole in the top plate. The steel ring was independent of the corrugated steel casing. The steel ring ensured that any movement of the casing as a result of soil compression from the bladder system or compaction of the soil during placement would not negatively affect the ability to inflate the bladders to the desired pressure.

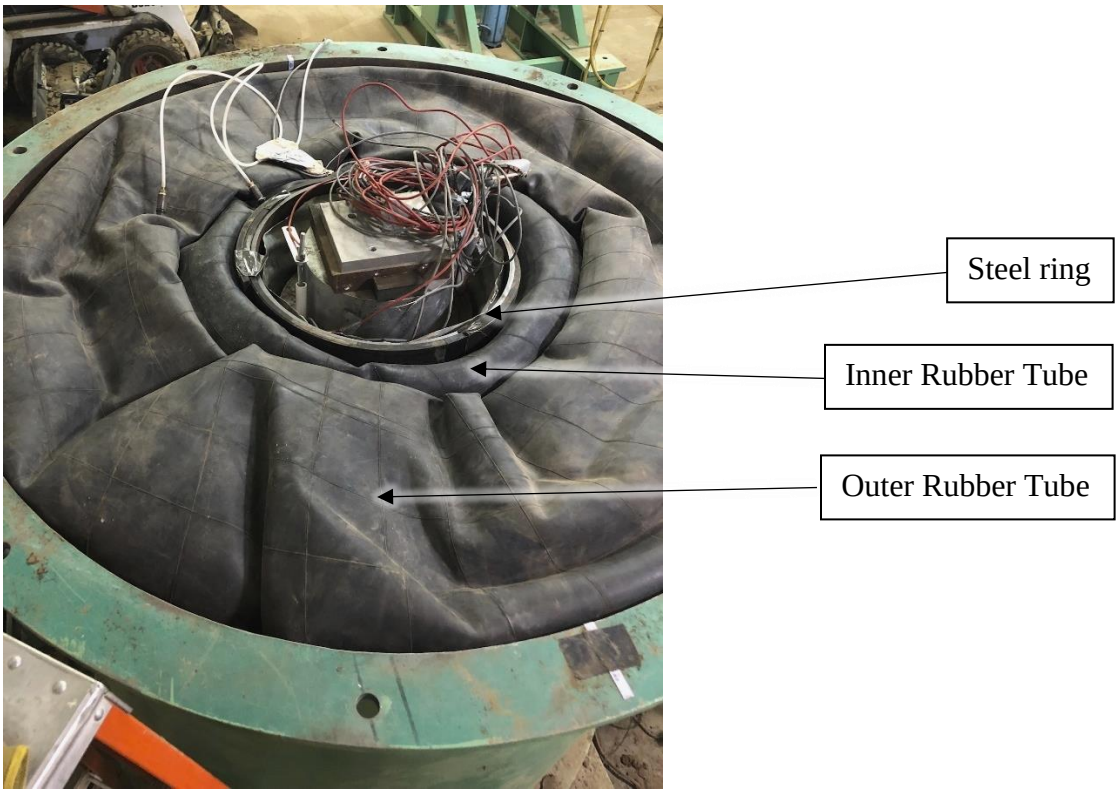

Figure 3.4 Bladder system showing the steel ring, inner rubber tube and outer rubber tube

The bladder system was connected to an Omega PX302-100GV pressure transducer, Fairchild high precision pneumatic pressure regulator and building air supply with ¼-inch OD polyethylene tubing. The pressure transducer was connected to both tubes inside of the chamber and could be read electronically. Figure 3.5 includes of the pressure transducer and pressure regulator. The pressure regulator was outside of the chamber and used to regulate the pressure entering the bladder system from the building air supply. Air from the building can reach peak pressures of 100 to 110 psi. Figure 3.6 is a schematic of the pressure control system used in a typical test. The regulator is outside the experimental apparatus and allows for adjustments within 0.1 psi. Pressurized air is sent through the regulator into the chamber assembly. The air is directed into two rubber tire tubes and also to a pressure transducer that is read by a computer during testing. The readings on the pressure transducer and the pressure gage on the pressure

regulator were observed during testing to determine any pressure loss along the tubing. In general, the electronic reading on the pressure transducer was within 0.1 to 0.5 psi of the pressure regulator. The pressure transducer reading was used to determine the actual applied pressure as it was connected directly to the tubes within the chamber.

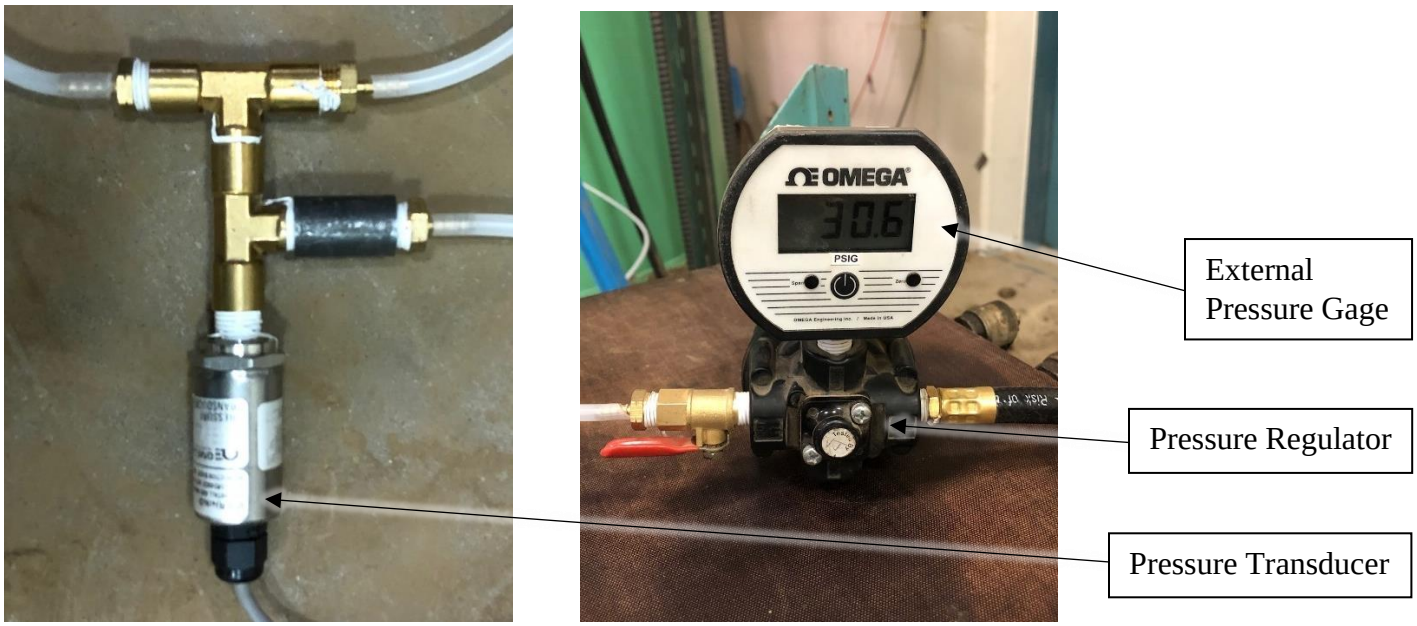

Figure 3.5 The pressure transducer, pressure gage and pressure regulator used to regulate and measure air pressure in the bladder system

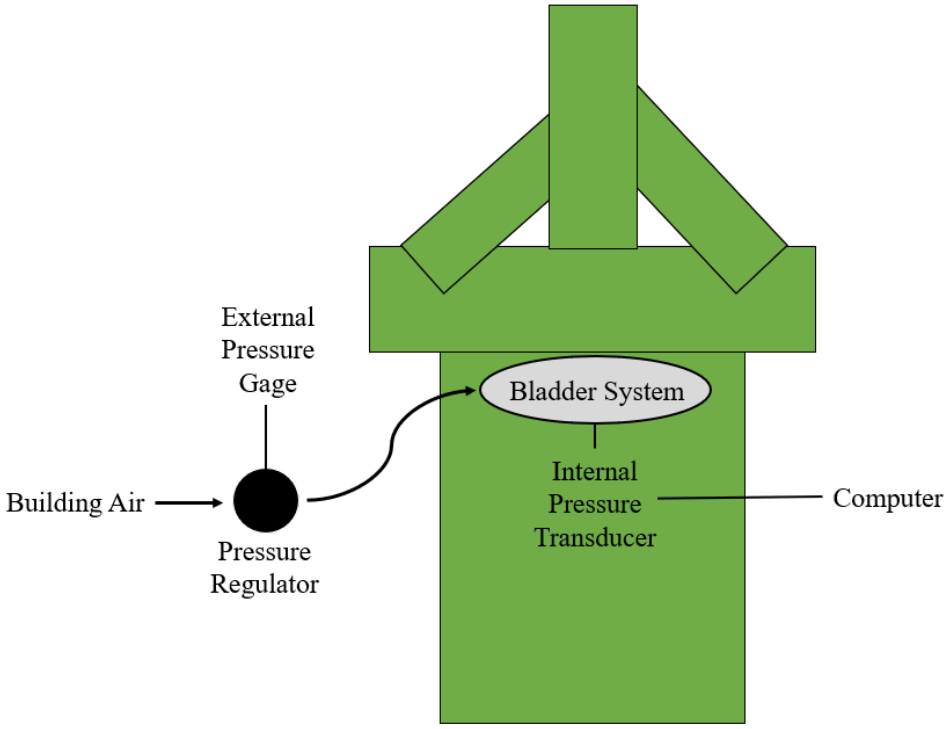

Figure 3.6 Schematic of the pressure control system detailing building air, pressure regulator, external pressure gage, bladder system, internal pressure transducer and computer

3.3 Model Drilled Shaft Foundation

A model drilled shaft foundation was used in this testing program to simulate the behavior a typical drilled shaft foundation in a laboratory setting. The goal of this research was to examine soil behavior and not other factors in involved in drilled shaft construction. For this reason the model foundation was precast and used for multiple tests. The model foundation consists of concrete, a steel rebar cage, strain gages and telltale tubes. The final precast foundation measured 16 inches in diameter and 28 inches tall.

The concrete mix design used for the model foundation is summarized in Table 3.1. The concrete mixture had a slump of nine inches with a water to cement ratio of 0.49. The model foundation was cast in a commercial grade Sonotube embedded in clean sand for lateral support

during curing. A concrete vibrator was used during placement to ensure the concrete filled all void space. The 28-day compressive strength was measured to be 5600 psi (Figure 3.7).

Table 3.1 Concrete mix design for model drilled shaft foundation

Parameter	Quantity
Portland Cement (lb.)	113.1
Fine Aggregate (lb.)	108.8
Coarse Aggregate (lb.)	240.9
Water (lb.)	56.1
Water Reducer (ml.)	132.1

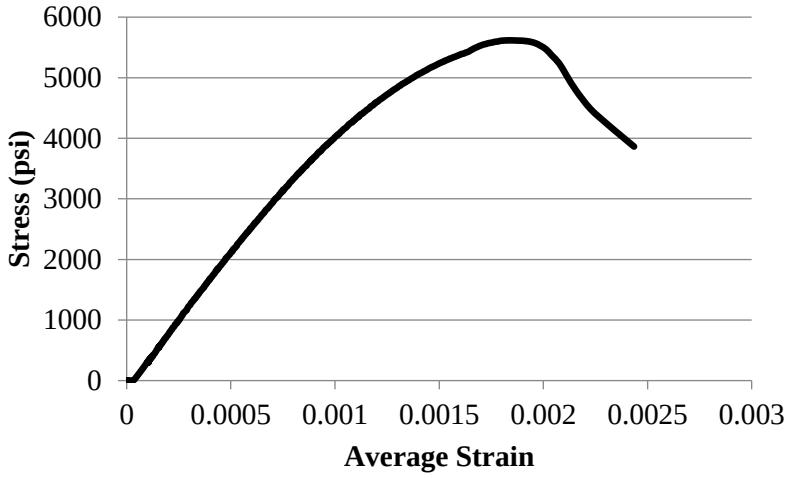

Figure 3.7 Results from uniaxial compression test on concrete used with model drilled shaft foundation

Figure 3.8 shows a side view of the model drilled shaft foundation prior to being cast in concrete. A rebar cage was constructed using a 1/16-inch wire mesh with 3-inch by 6-inch openings. The rebar cage is 12 inches in diameter and designed to have 2 inches of concrete cover. Additionally, ten No. 4 reinforcing bars were attached to the wire mesh to achieve a steel reinforcement ratio of 1.1 percent. Two 1-inch outside diameter (OD) PVC tubes were attached

on opposite sides of the outside of the rebar cage. A 5/16-inch diameter threaded rod was placed inside the PVC tube with an oversized washer anchored in the concrete at the base of the model foundation. Measurements of displacement from the bottom of the foundation can be taken from these telltale rods at the exposed top of the foundation.

Two vibrating wire strain gages and four electrical resistance strain gages were cast into the base of the foundation. A photograph of the strain gages before placing concrete can be seen in Figure 3.9. The strain gages were evenly spaced around the inside of the reinforcing cage approximately five inches from the side of the model and 3 inches from the base. They were attached to standard metal U bolts which were attached to the reinforcing cage. The electrical resistance strain gages proved to be an unreliable method for measuring strain due to the variability in output and were not used. Figure 3.10 shows the completed model drilled shaft foundation.

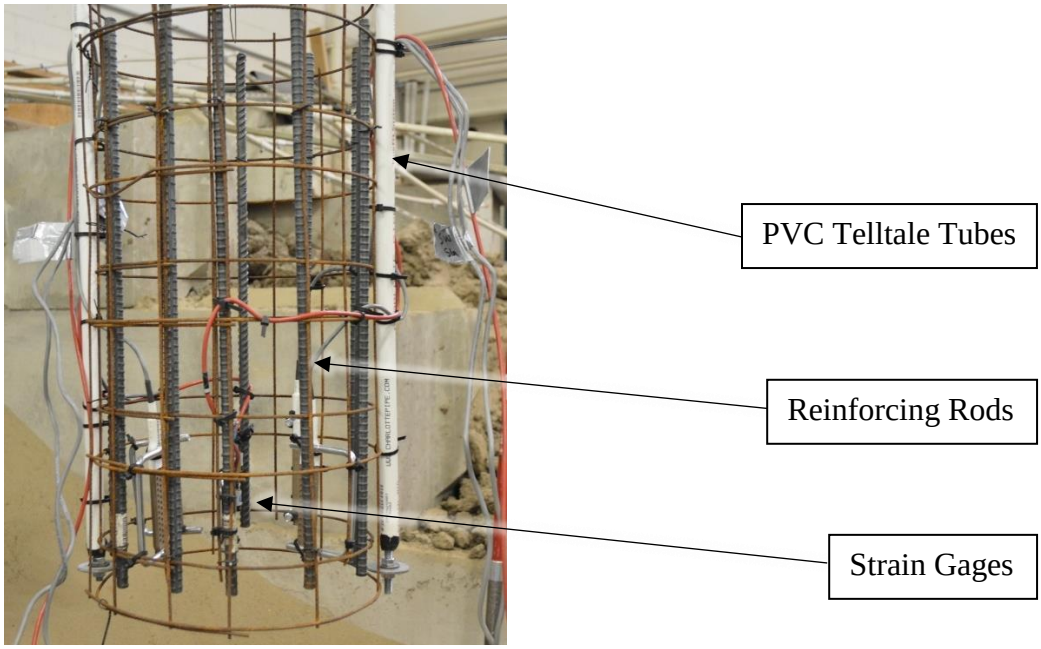

Figure 3.8 Rebar cage with PVC telltale tubes, reinforcing rods and strain gages

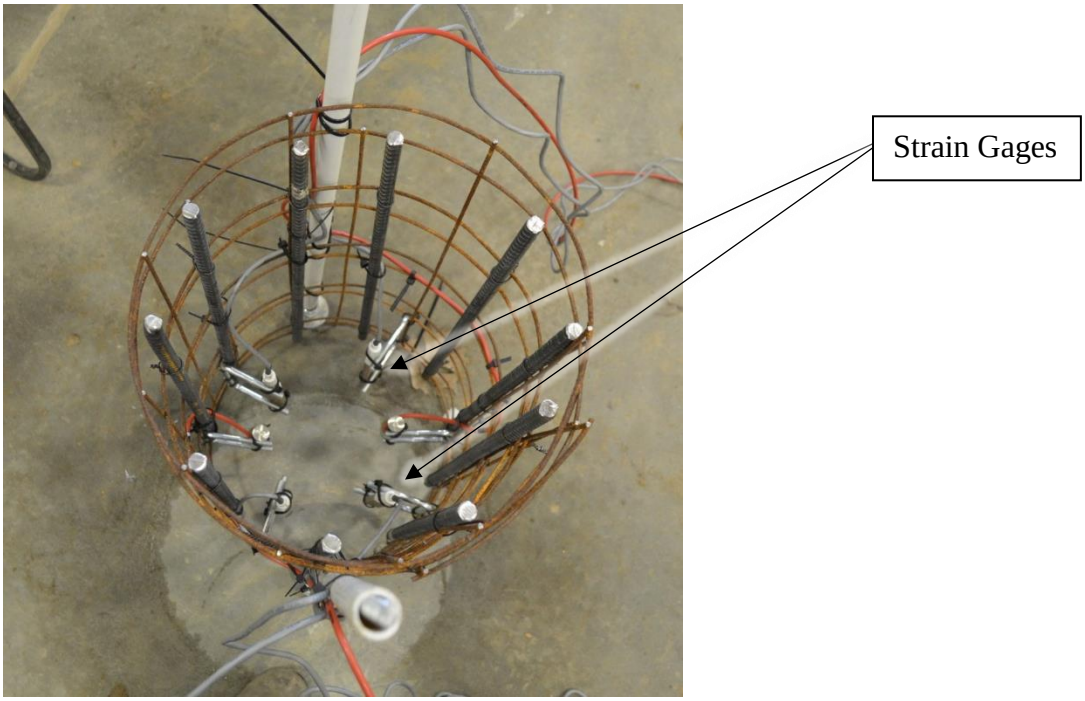

Figure 3.9 Rebar cage from above showing the locations of the strain gages within the model foundation

Figure 3.10 Final model drilled shaft foundation used during testing

3.3.1 Casing

To eliminate side resistance and isolate load-settlement behavior at the tip of the model drilled shaft foundation, a casing was implemented. Some tests utilized a casing and some tests did not. The use of a casing is discussed on a test-by-test basis in Chapter 4.

A variety of casings were evaluated including a high strength commercial grade Sonotube™. Numerous problems presented themselves mainly near the free end of the Sonotube™ where pressure from the bladder system was applied to the walls of the tube. Figure 3.11 shows two different methods used to reinforce the Sonotube™ casing. Several attempts were made to reinforce the free end of the Sonotube™ with a 2-inch thick Styrofoam Utilityfit 15 psi scored insulation board and 11/16-inch thick plywood board but were ultimately unsuccessful.

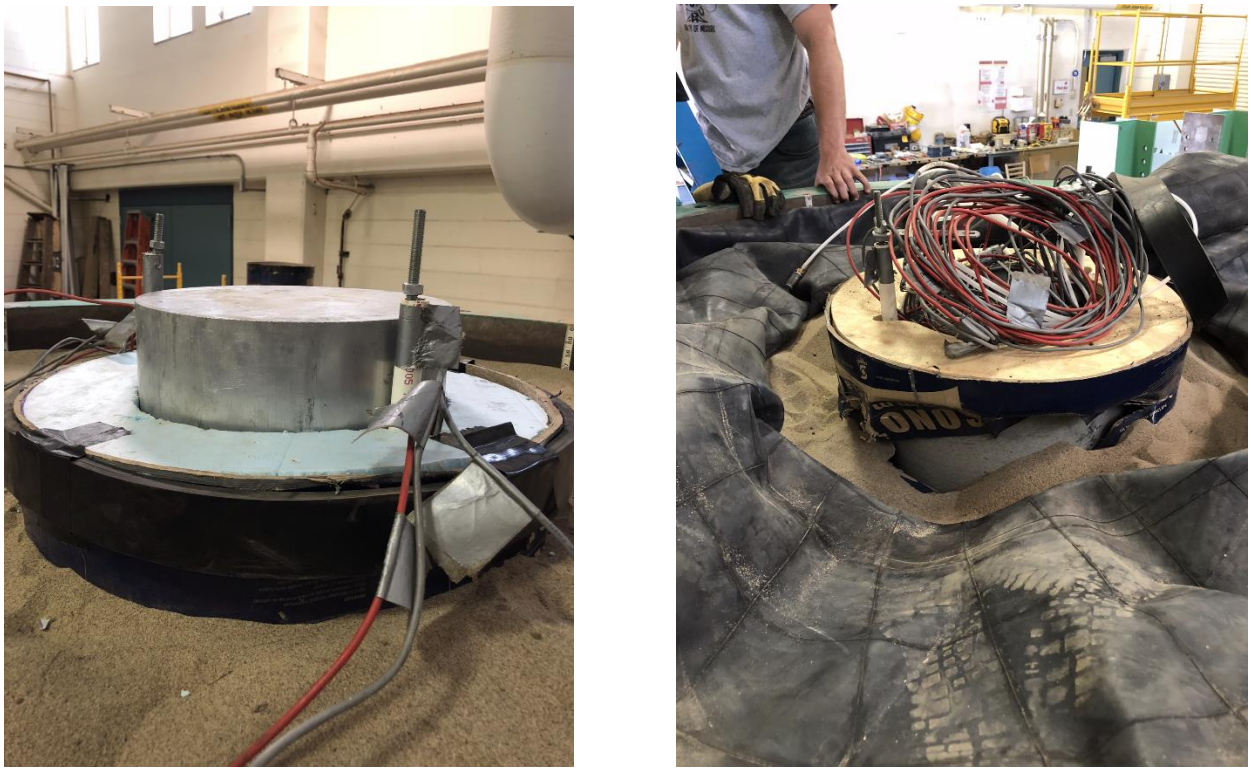

Figure 3.11 Reinforcement used to support the free end of the commercial sonotube casing

An 18-inch diameter by 31 inches tall corrugated steel pipe with an 1/8-inch wall thickness was used as a casing sucessfully. Figure 3.12 includes a photo of the corrugated pipe and Figure 3.13 shows a photo of the casing and steel pipe mentioned previously in Section 3.2. The corrugated steel pipe surrounds the model foundation and eliminates side resistance. The casing isolates interaction between the soil and the tip of the model foundation. The steel casing was strong enough in compression to resist the forces applied by the bladder system.

Figure 3.12 Corrugated steel pipe used as a casing in this testing program

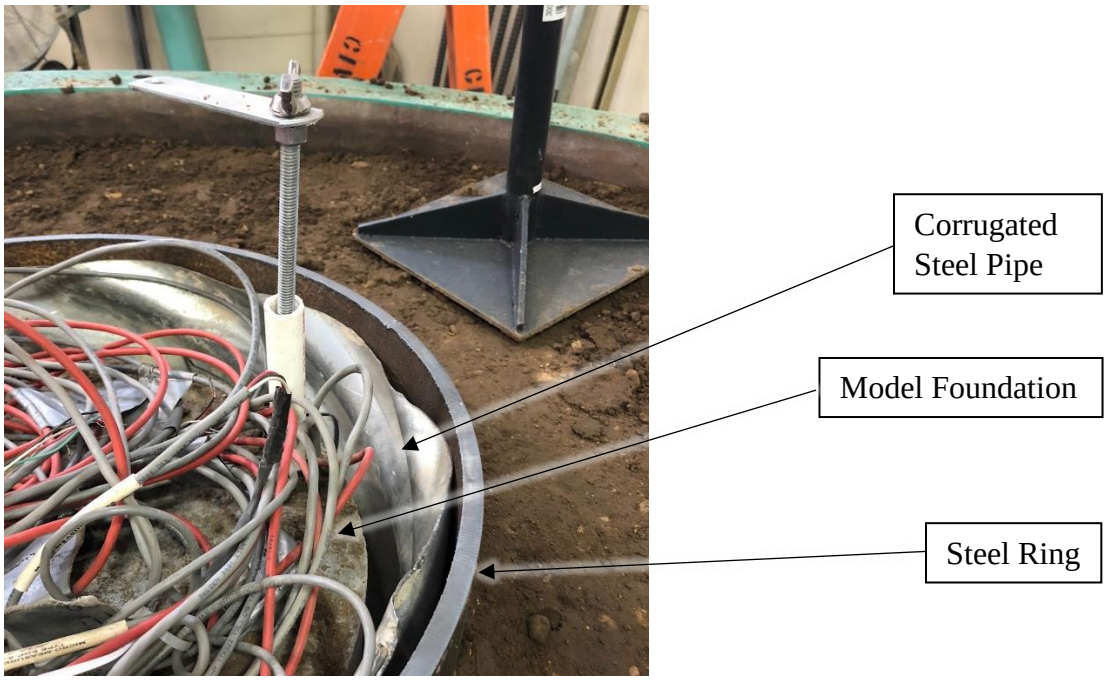

Figure 3.13 Corrugated steel casing and the steel pipe in the calibration chamber with the model foundation prior to testing

3.3.2 Aluminum Load Transfer Cylinder

A 6-inch tall, 12-inch diameter aluminum cylinder was centered on top of the model foundation during testing. A photograph of the aluminum cylinder is shown in Figure 3.14 Presently, the hydraulic jack used to apply load to the model foundation has a 4-inch by 4-inch steel plate attached to the bottom of the piston. The aluminum cylinder was used to uniformly distribute load to the model applied by the hydraulic jack.

Figure 3.14 Aluminum cylinder used in this testing program

Discrepancies in displacement of the top versus tip of the foundation as a result of strain of either the concrete or aluminum cylinder are small enough to be neglected at the loads used in this test. The modulus of the concrete in the shaft is 4414 ksi, likewise the modulus of the 12-inch diameter by 6-inch long aluminum cylinder used to transfer load to the foundation is 10,000 ksi. Shortening of either of these materials at the highest loads tested in this testing program, 70.3 kips, would be equal to 0.0026 inches. Relative variability in the measurement of

displacement due to rotation of the foundation outweigh a concern for inaccuracy in displacement due to the materials used in the testing program.

3.4 Soil Properties

Two types of soil were used in this laboratory testing program: a poorly-graded clean sand and a poorly-graded silty sand. Both soils were dredged from the Missouri River near Jefferson City, Missouri. A series of tests were performed to characterize both soil types, as described in the following sections.

3.4.1 Poorly Graded Sand

A series of index tests were performed on samples of poorly graded sand used in this laboratory testing. A summary of the results is shown in Table 3.2. In addition to index tests, multiple drained direct shear tests were performed. The angle of internal friction from this test the was determined to be 39 degrees. A summary of the test results can be seen in Figure 3.16.

Table 3.2 Summary of results of index tests on poorly graded clean sand

Parameter	**Value**	**Test Method**
Soil Classification	SP	ASTM D2487-17
Fines Content (percent passing #200 sieve)	2.3%	ASTM D422
Maximum Unit Weight, $\gamma_{d,\,max}$	107.7 pcf	ASTM D4253
Minimum Void Ratio, e_{min}	0.57	
Minimum Unit Weight, $\gamma_{d,\,min}$	91.2 pcf	ASTM D4254
Maximum Void Ratio, e_{max}	0.85	
Average Placement Water Content, w_c	0.31%	ASTM D2216
Angle of Internal Friction, ϕ	39°	ASTM 6528
Cohesion Intercept, c	0 psf	

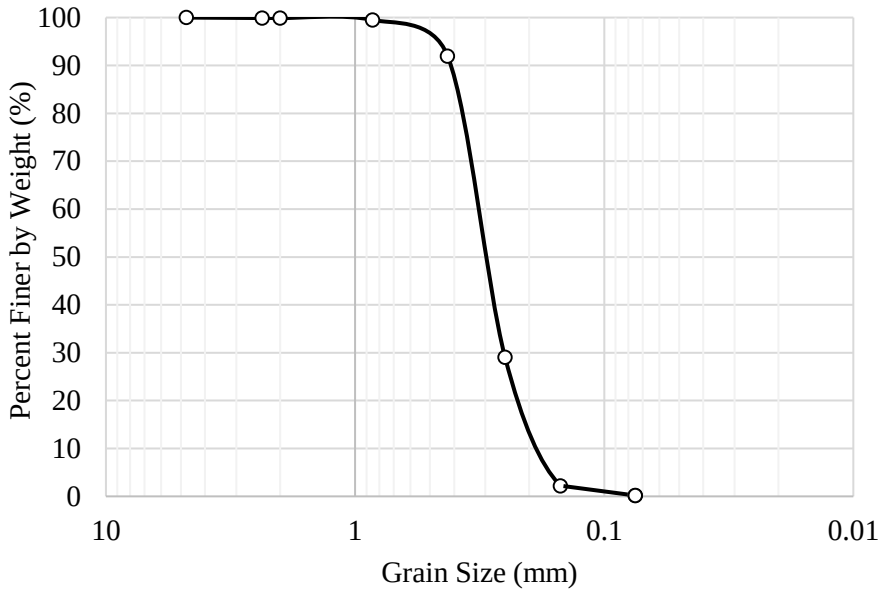

Figure 3.15 Grain size distribution for poorly graded clean sand (SP)

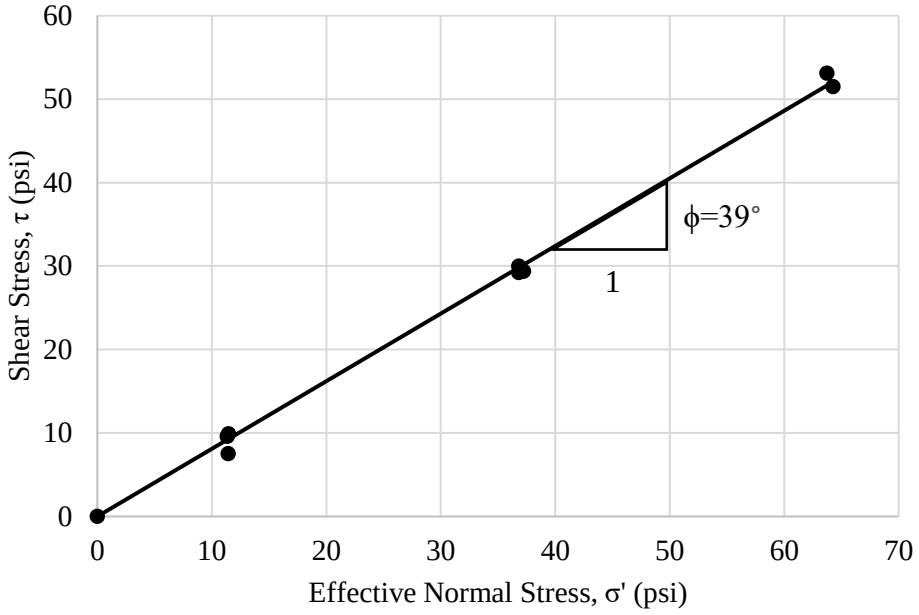

Figure 3.16 effective stress failure envelope for poorly graded clean sand (SP) from direct shear tests

3.4.2 Silty Sand

A series of index tests were performed on samples of silty sand used in this laboratory testing. A summary of the results can be found in Table 3.3.

Table 3.3 Summary of results of index tests on silty sand

Parameter	**Value**	**Test Method**
Soil Classification	SM	ASTM D2487-17
Fines Content (percent passing #200 sieve)	18.8	ASTM D422
Optimum Water Content, w_{opt} (%)	9.3	ASTM D698-12e2
Maximum Dry Density, $\gamma_{d,\,max}$ (pcf)	125.0	

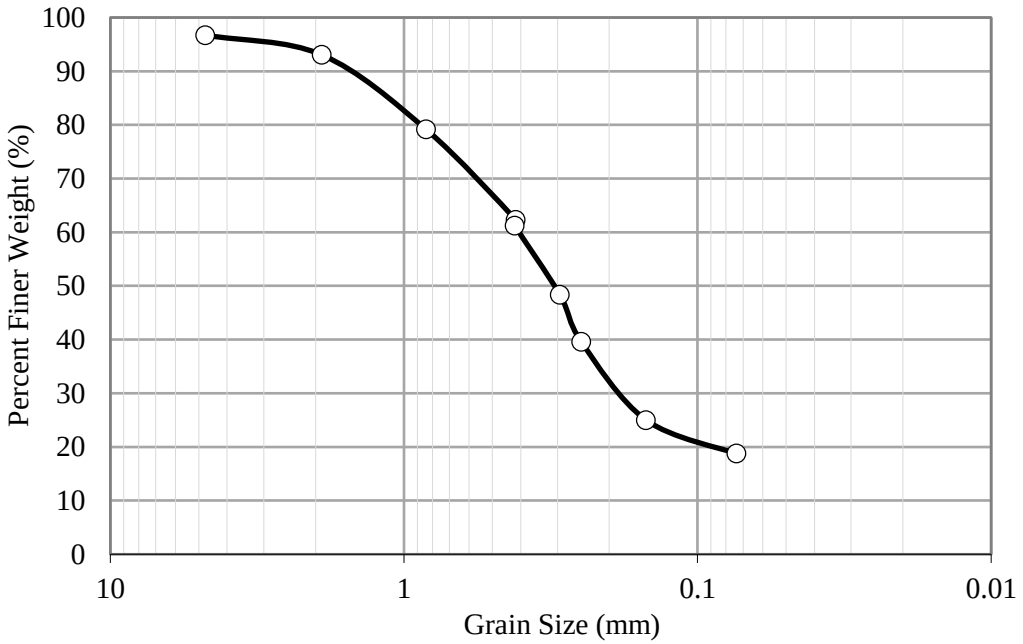

Figure 3.17 Grain size distribution for silty sand (SM)

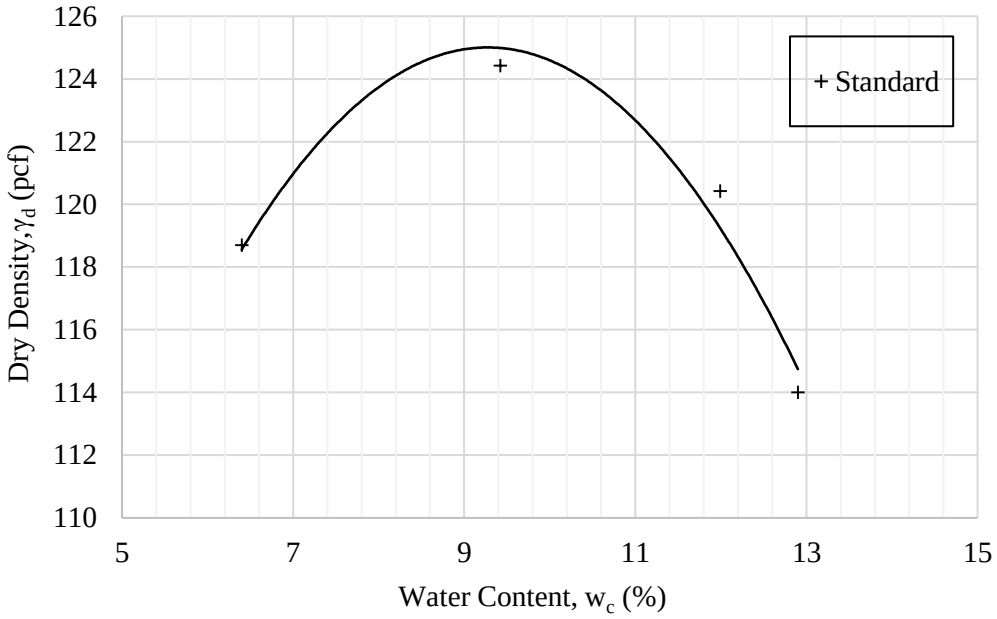

Figure 3.18 Results from standard proctor test performed on silty sand (SM)

The workability and strength properties of the silty sand vary greatly with water content. Compacting the soil 1-2% wet of the optimum water content was determined to be the best setup for workability and repeatability.

The compacted silty sand presented several issues with consolidation of the soil during inflation of the bladder system. Compared to the poorly graded sand, the silty sand required significantly more time to consolidate. The same testing procedure described in Chapter 3 was utilized for tests on the silty sand. The main difference was monitoring during and after inflation of the bladder system required more attention. Compared to the poorly graded sand which consolidated in a short period of time the silty sand required several hours until it could be determined that the consolidation of the soil was complete. Figure 3.19 shows an annotated example of a plot of displacement measured from LVDTs on the foundation versus time.

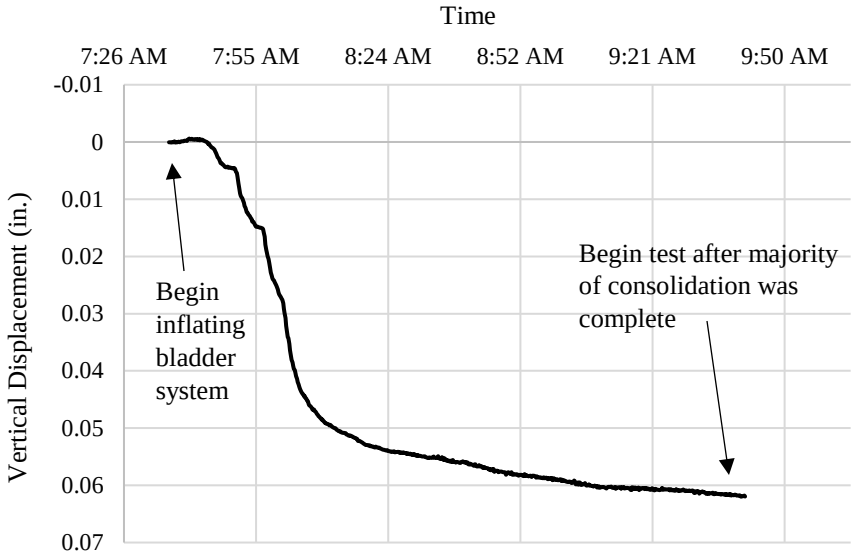

Figure 3.19 Vertical displacement versus time for the foundation immediately following inflation of the bladder system prior to testing

3.5 Instrumentation

Instrumentation was used with the experimental apparatus to measure four performance measures: (1) axial load applied to model shaft; (2) air pressure in the bladder system; (3) vertical movement of the shaft; and (4) strain at the tip of the foundation under axial load. The initial and final density of the soil for each test were also evaluated using density tins, water balloon density tests, and by weighing the amount of soil placed for each test.

3.5.1 Load Measurement

Axial load was measured using a Lebow Associates, Inc. Model 3117-106 load cell. The maximum capacity of the load cell is 150,000 lbs (150 kip). Figure 3.20 shows the output voltage from the load cell versus load. The load cell was calibrated for repeatability and linearity in a Tinius Olsen Universal Testing Machine by reading voltage output from the load cell when subjected to known forces from the testing machine.

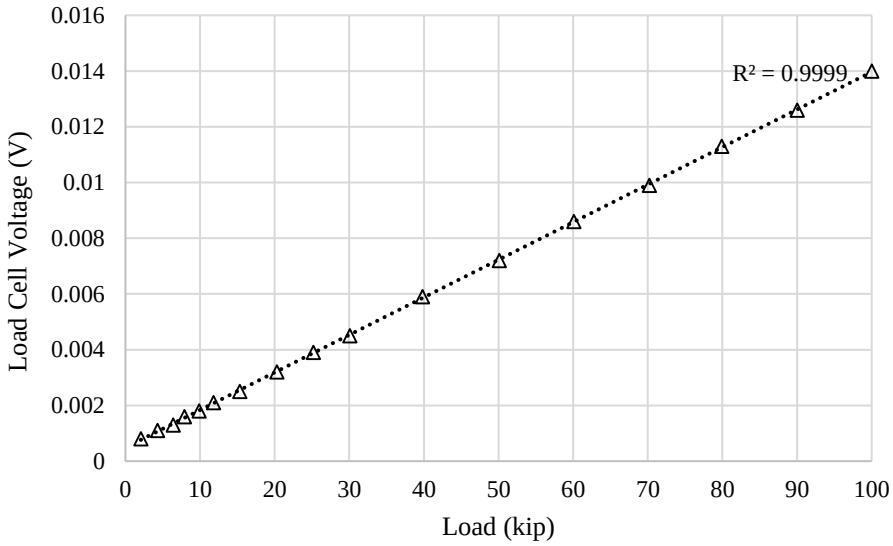

Figure 3.20 Load cell calibration showing the output voltage versus applied force

The hydraulic pressure applied to the hydraulic pump was used as a secondary check of accuracy of the load cell. The pressure was measured at various load steps during testing using a pressure gage attached to the hydraulic pump. The data shown in Figure 3.21 is taken from the testing program using the load cell and hydraulic pump. The measured hydraulic pressure was plotted against the load output from the load cell.

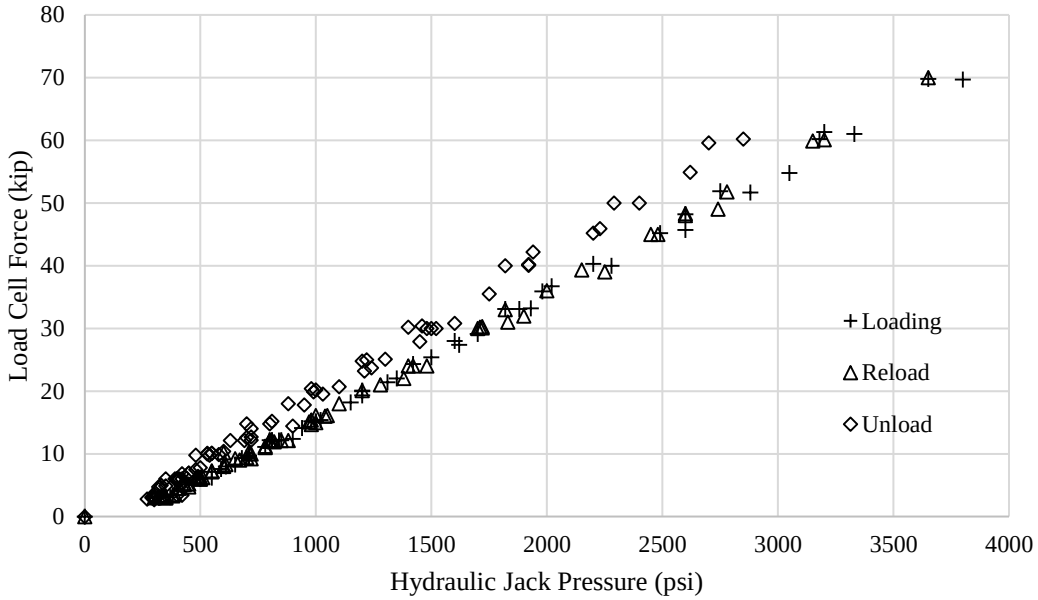

Figure 3.21 Hydraulic jack pressure versus load cell readings from all tests in the testing program

3.5.2 Air Pressure

Air pressure in the bladder system was recorded using a pressure transducer connected to a data recording system as mentioned in Section 3.2. The measurement was used to determine the effective overburden stress applied to the soil. The target range for the tests performed in this testing program was between 10 and 30 psi. This range of pressures allows for pressure simulation in the range of 10 to 70 feet below the ground surface.

3.5.3 Vertical Displacement Measurement

Vertical displacement of the model shaft was measured using a combination of dial gages and linear variable differential transducers (LVDT). One dial gages was used to measure vertical movement of the shaft. A small camera was setup near the dial gage to read the values from a safe distance. Four LVDTs were used to measure displacement of the top and bottom of the shaft.

Two of the LVDTs were placed on the top of the foundation, typically on opposite sides of a 12-inch diameter by 6-inch tall aluminum cylinder used to uniformly distribute load from the hydraulic jack to the model shaft. A schematic showing the placement of the LVDTs on the top of the model foundation can be seen in Figure 3.23. Two additional LVDTs were placed on metal risers attached with winged nuts to the threaded rod anchored in the base of the shaft. Three of the LVDTs, both top of shaft LVDTs and one of the bottom of shaft LVDTs, in addition to the dial gage were attached to an independent reference frame to ensure their measurements were independent of any movement of the experimental apparatus. A photo detailing the independent reference beam and several of the LVDTs can be seen in Figure 3.22. The reference beam was constructed of UNISTRUT in such a way that it was not in contact with the experimental apparatus. The remaining LVDT, which measured movement near the base of the shaft, was attached to a magnetic holder which rested on the reaction frame of the experimental apparatus. In some tests, the dial gage was attached to a magnetic holder. The dial gage only served as a manual check during testing to determine an approximate magnitude of displacement. Data from the dial gage was not included in any results or used to make any conclusions relating to this project.

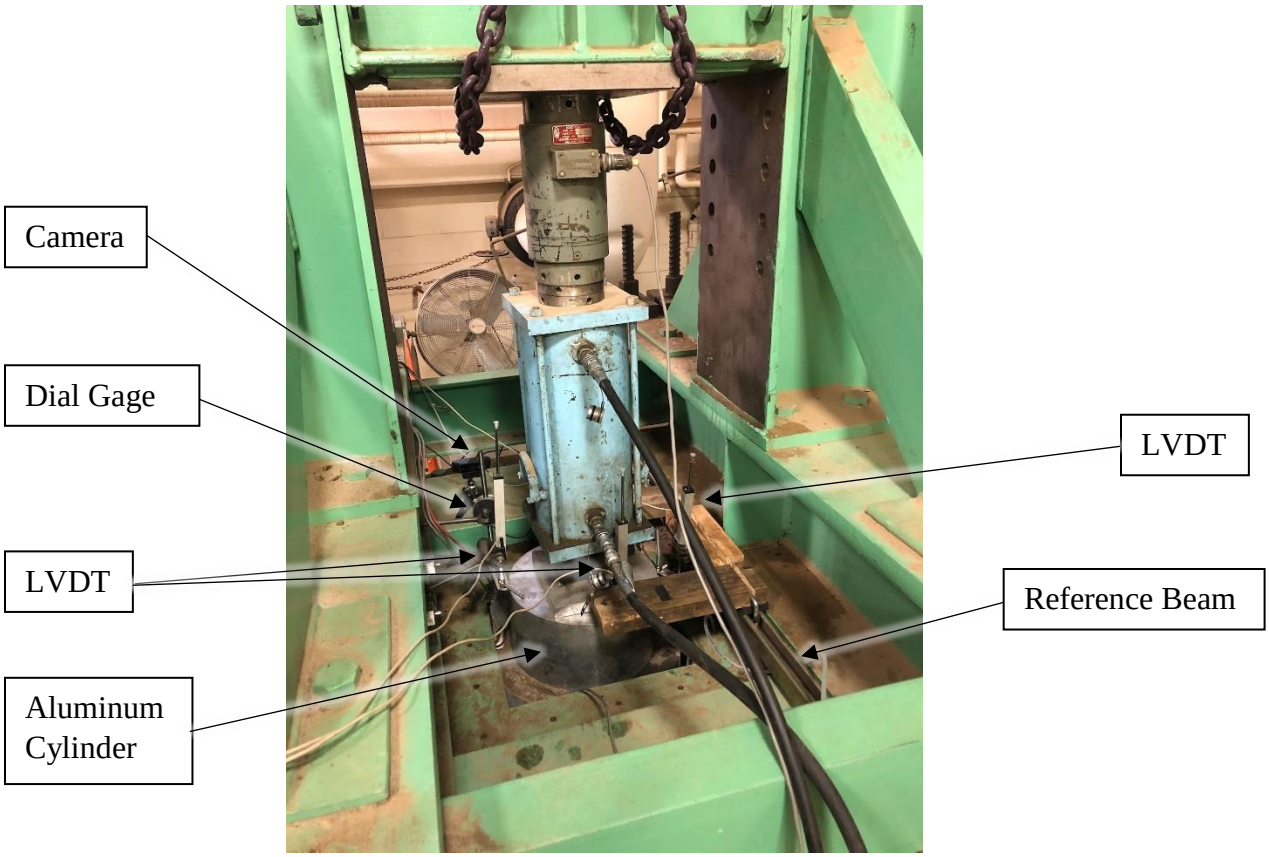

Figure 3.22 Reference beam, camera, dial gage and LVDT placement in a typical test

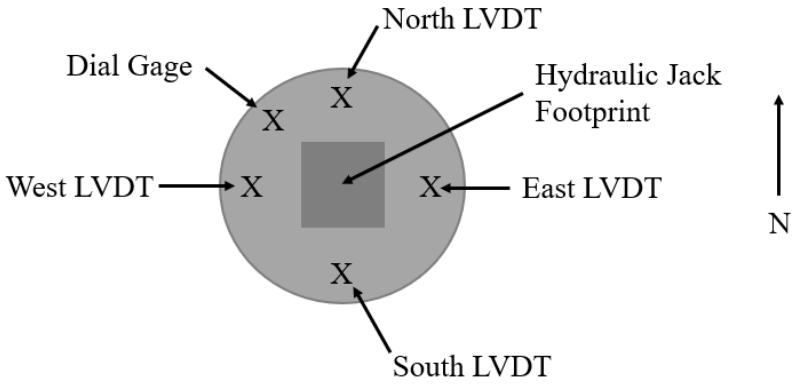

Figure 3.23 Schematic showing the LVDT and dial gage placement on the top of the model foundation in a typical test

3.5.4 Model Shaft Strain Measurement at Foundation Tip

A total of six strain devices were cast into the model drilled shaft. Two Geokon™ Series 4200 vibrating wire strain gages were installed on opposite ends of the foundation approximately three inches from the base of the foundation. Measurements for the vibrating wire strain gages were collected using a Geokon™ 16 channel multiplexer connected to a laptop computer which monitored and recorded the data in LogView.

The model foundation was calibrated in an overhead press capable of applying axial load up to 300 kips. A load cell attached to the overhead press allowed for calibration of the model foundation and the strain gages embedded in the concrete. Figure 3.24 shows the calibration of strain gage voltage versus axial load from the load cell attached to the overhead press. The calibration showed a linear relationship between vibrating wire strain gage voltage and applied axial load. Calibration of the model foundation allowed for strain measurement during testing. Due to the relatively small loads applied to the foundation during testing, Hooke's Law can be used to estimate the applied axial load near the base of the model foundation. During testing, readings from the strain gages can be used to determine applied axial load or as a secondary check of the load cell attached to the experimental apparatus.

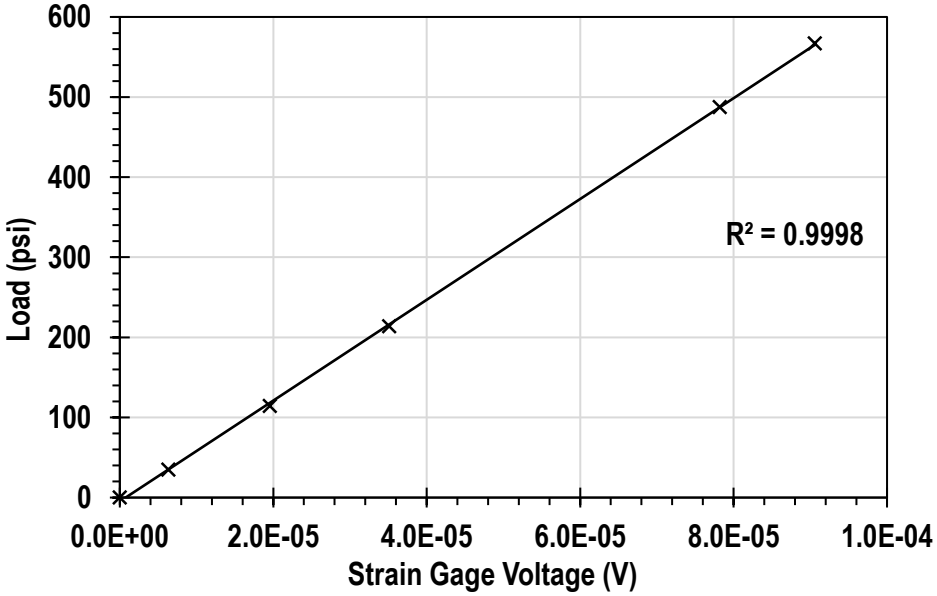

Figure 3.24 Calibration of vibrating wire strain gages in the model foundation versus load

Four electrical resistance strain gages were cast in opposite quadrants of the base of the shaft approximately three inches above the base. The electrical resistance strain gages were connected to a panel board and read using a LabVIEW program on a computer. The four electrical resistance strain gages installed near the base of the foundation were unusable in this project. They were cast into the foundation with the goal of recording more data points in a shorter interval compared to the vibrating wire strain gages. Although they provided the ability to collect more data points, the variability and unreliability did not allow for any data to be used in this testing program.

3.5.5 Soil Density Measurement

The density of the soil in the test chamber was measured in three different ways. In the tests conducted using poorly graded sand, density was recorded using density tins. In the silty sand tests the density was measured using the rubber balloon density test. The weight of soil

placed in the chamber for each test was also recorded to provide an independent assessment of the average density for the entire test chamber.

The density tins used in this laboratory testing were placed in the poorly graded sand prior to testing. A photograph of a typical density tin is shown in Figure 3.25. The density tin was used to measure soil density after overburden stress was applied to the soil. The density tins occupy a measurable volume and weight when filled with soil. The weight of the density tin divided by the known volume provides and estimation of the final unit weight of the soil. A variety of tin sizes were used ranging from 1.75 to 2.5 inches in diameter and 2.5 to 3.5 inches in height. The density tins were removed at the conclusion of testing during the excavation phase. In order to prevent disturbance, zip ties were attached to the tins and used to detect and excavate the tins. Extreme care was taken during excavation, but some disturbance occurred. Heavily disturbed samples were not used to determine the final soil density.

Figure 3.25 Typical density tin used to determine final density of the poorly graded clean sand

Initial and final density measurements for the silty sand were determined using the rubber balloon density test. Figure 3.26 shows a schematic drawing and principle of the rubber balloon test from ASTM D2167-15. The test was performed in accordance with ASTM D2167-15. The test uses a liquid-filled vessel to fill a rubber membrane to determine the volume of a small excavated hole. The initial volume of the flat surface and the final volume of a small excavated hole is recorded. The weight of the excavated soil is also recorded. The recorded weight divided by the difference in the initial and final volumes produces the total unit weight.

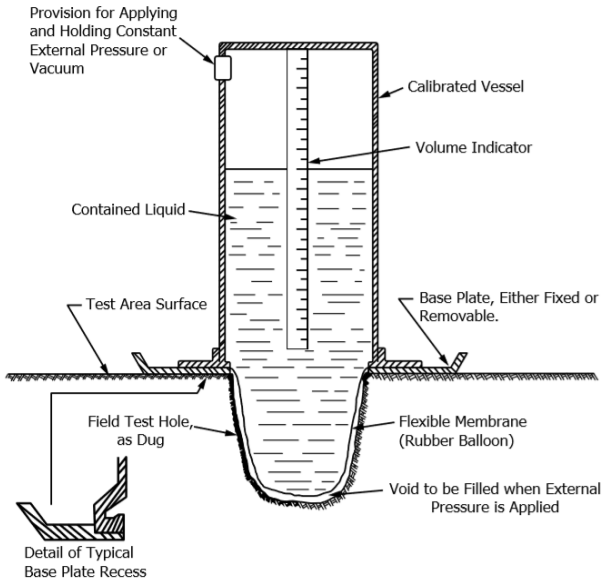

Figure 3.26 Schematic of vessel and principle of the rubber balloon test used to determine in-situ density of the compacted silty sand (ASTM D2167)

The weight of the soil placed into the chamber for each test was recorded to provide an independent assessment of the average density for each test. Figure 3.27 is a photograph of the GAR-BRO dump bucket attached to the KLAU crane scale attached to the 10-ton overhead crane. The weight of soil placed was measured using a KLAU OCS-S1 crane scale with a 2000 lb. capacity. The scale attaches to a GAR-BRO type 413-R, 3-foot diameter dump bucket and to

a 10-ton capacity overhead crane. The total unit weight was determined by summing the weights from each dump bucket and dividing by the volume of the chamber.

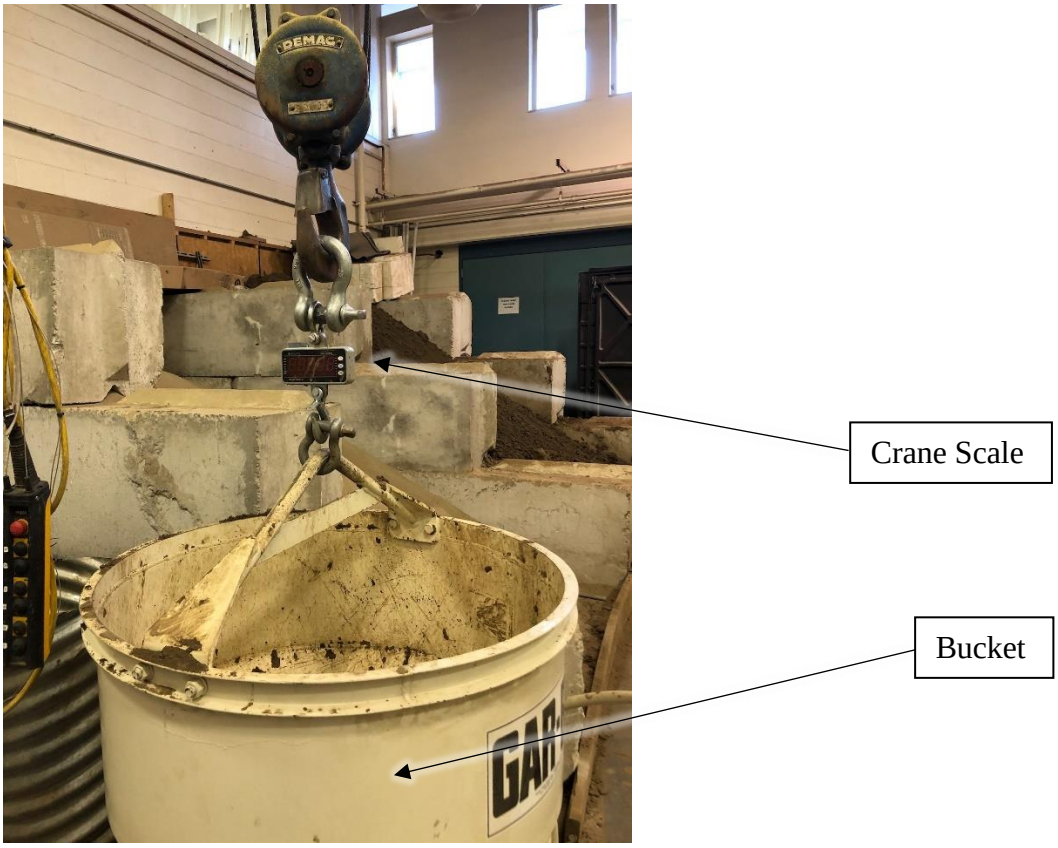

Figure 3.27 GAR-BRO dump bucket and KLAU crane scale

3.6 Testing Procedure

The experimental procedure followed during testing involves three main steps: (1) experimental setup including model drilled shaft foundation, soil, casing, and bladder system; (2) testing at a specific vertical effective stress; and (3) disassembly of the experimental apparatus. Each phase of the testing procedure is described in more detail in this section.

3.6.1 Experimental Setup

The following steps were performed to setup the experimental apparatus for testing;

1. Remove any excess soil or debris from the chamber
2. A Bobcat 465 skid steer loader with a bucket attachment was used to fill a 3-foot diameter dump bucket with either poorly graded clean sand or silty sand
3. The dump bucket and soil were weighed using a crane scale and recorded
4. Samples from each bucket were collected to determine the water content of the soil.
5. The dump bucket was lifted into the testing chamber using a 10-ton overhead crane. In tests with poorly graded sand a pluviation device was attached to the underside of the dump bucket. The pluviation device has two levels of sieves that promote particle scattering and uniform soil placement within the chamber.
6. The soil was deposited into the chamber from a height of 24 inches.
7. In the tests where a loose configuration was desired, the soil was not compacted. In tests were a dense configuration was desired the soil was spread into approximately six-inch lifts and compacted using a 10-inch by 10-inch square flat plate tamper in a circular pattern to ensure uniform compaction.
8. In tests with poorly graded sand, density tins were placed at three different heights in the chamber. The tins were placed approximately 18 inches, 30 inches and 48 inches from the base of the chamber. Four density tins were placed at each height in each quadrant surrounding the model foundation. The tins were approximately six inches from the edge of the chamber.
9. In tests with silty sand, rubber balloon density tests were performed to determine the placement density of the soil.

10. Once the soil level reached approximately 32 inches from the bottom of the chamber the corrugated steel casing was placed. Using a measuring tape and level the casing was moved into the correct position at the center of the chamber.
11. Using the 10-ton overhead crane the model foundation was lifted into the chamber and placed in the corrugated steel casing.
12. After the casing and foundation had been placed, the remaining soil was added. Periodic checks were made with a tape measure and level to ensure the casing or foundation did not move as more soil was added.
13. The chamber was filled to leave a three-inch gap between the top of soil level and the underside of the chamber lid.
14. Figure 3.X shows how a 19-inch diameter, 6-inch long, 3/8-inch thick steel pipe was fit around the outside of the corrugated steel casing.
15. The bladder system was placed in the void space between the top of soil and underside of the chamber lid. Polyethylene tubing and wires connecting to the pressure transducer inside the chamber were threaded through small holes in the chamber lid and connected to the pressure regulator and data acquisition system respectively.
16. Using the 10-ton overhead crane the top lid was lifted into place. The lid was connected to the chamber assembly using A325 bolts with locking washers.
17. Using the bobcat loader the aluminum cylinder as seen in Figure 3.X was placed on top of the model foundation.

18. Using the 10-ton overhead crane the reaction frame consisting of the hydraulic jack and load cell was placed on top of the top lid. Eight DWIDAG bars were installed to secure the reaction frame to the bottom assembly.
19. An independent reaction frame was moved into position between the top lid and the reaction frame. Figure 3.X shows the reaction frame with instrumentation attached.
20. The bladder system, load cell, and strain gages were connected to a data acquisition device. A camera was connected to a computer and placed near the hydraulic jack to monitor a dial gage. Hydraulic hoses were connected to the hydraulic jack and hydraulic pump.
21. Zero readings were established from a LabVIEW computer program used to record data points from LVDTs, pressure transducers and electronic strain gages.
22. Baseline values were recorded from the vibrating wire strain gages using a 16-channel logger and computer.
23. The bladder system was inflated using a pressure regulator and building air supply to the desired vertical overburden pressure. Testing was performed at various pressures ranging from 10 to 30 psi.
24. The pressure in the bladder system was increased slowly over the course of 60 to 90 minutes to ensure the rubber tubes could fill all void space and not rupture prematurely. During this time LVDTs and a dial gage were monitored for movement.
25. Once the target pressure had been achieved, movement of the foundation was monitored.

3.6.2 Testing

The testing procedure involved several loading, unloading and reloading cycles. A typical test followed the following procedure;

1. The hydraulic pump was turned on and the jack was extended to just above the model foundation.
2. A seating load of approximately 3 kips was applied to the foundation.
3. Axial load was increased in steps to predetermined values based on anticipated settlement. The steps were determined based on previous experience and careful monitoring of the load-settlement data during testing.
4. During testing, the dial gage was monitored and recorded. The load was not increased to the next loading step until the dial gage and LVDT data had stopped moving. For tests with the poorly graded sand each loading step took approximately 3 to 5 minutes. For tests with the silty sand the loading step took 10 to 15 minutes.
5. After movement had stopped, the hydraulic pump was used to decrease the axial load on the model foundation. In all load steps, the model foundation was unloaded to zero.
6. Once the zero readings had been taken, steps 2 through 5 were repeated. Table 3.4 shows a table of a typical loading schedule used during testing. The number of load-unload-reload cycles vary by test and were dependent on the ultimate load, capacity of the hydraulic pump and magnitude of total displacement recorded throughout the test.

Table 3.4 Typical loading schedule used for a test showing individual load steps and axial load applied

Loading Step	Axial Load (kip)								
1	0	3	0						
2	0	3	6	3	0				
3	0	3	6	9	6	3	0		
4	0	3	6	9	12	9	6	3	0

7. The model foundation was reloaded to the previous maximum load. Figure 3.28 shows an annotated result with arrows showing the path of loading-unloading-reloading. After reaching the previous maximum load the axial load was increased to the next loading step before being unloaded as in step 5.

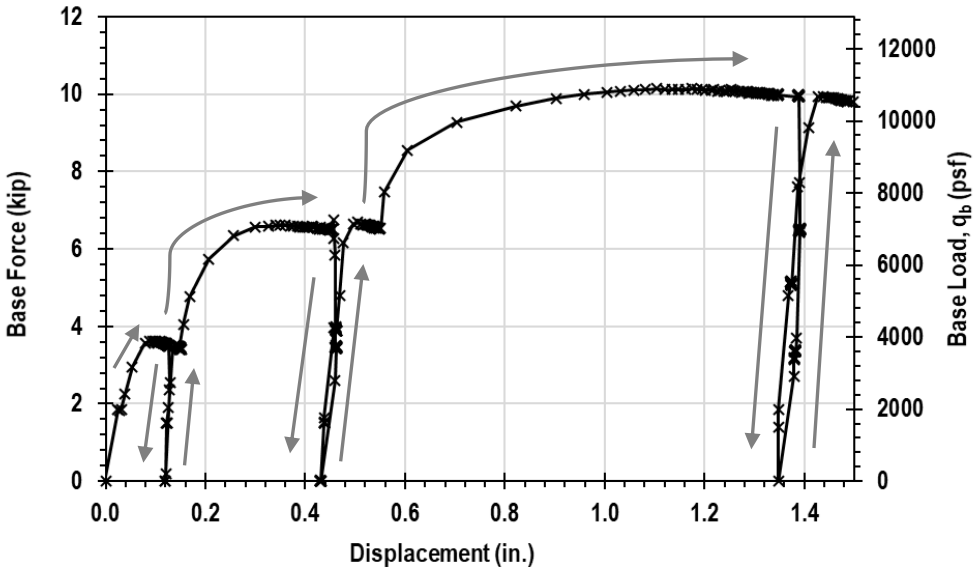

Figure 3.28 A typical load test showing an annotated path of loading, unloading and reloading

3.6.3 Disassembly

Disassembly following a test consisted of the following steps;

1. Pressure was released from the bladder system.
2. Instrumentation was removed from the independent reference beam and taken down.
3. A 10-ton overhead crane was used to remove the reaction frame and top lid.
4. The bladder system and model foundation were removed from the chamber.
5. The soil was excavated from the chamber. During excavation, soil density tins for tests in poorly graded clean sand were collected and recorded. In tests with silty sand, water balloon density tests were performed during excavation.

3.7 Summary

In this chapter, the experimental apparatus, model, medium and instrumentation used to evaluate the load-settlement behavior of a model drilled shaft foundation tip was described. The apparatus includes a chamber assembly, top and bottom plate and reaction frame. The model drilled shaft was described in detail including relevant material properties, and instrumentation within the model. The soil used in the testing program was described. The instrumentation used during testing including the bladder system, hydraulic system, LVDTs to measure vertical movement and load cell to measure axial load were described. The testing procedure including assembly, testing and disassembly of the experimental apparatus was also detailed.

Chapter 4 Testing Program and Results

The results of nine tests performed with a model drilled shaft foundation in coarse grained soils. A summary of the testing program is presented in addition to axial load-displacement plots from nine individual tests. Additional information about setup is presented on a test-by-test basis and includes soil type, dry unit weight, relative density and average water content. The measured average overburden pressure applied by the bladder system is included for each test and plotted versus time.

4.1 Testing Program

A total of nine axial-load displacement tests were performed in three different soil configurations. The testing program is organized into three sections based on soil configuration. The soils tested were loose poorly graded clean sand, dense poorly graded clean sand and compacted silty sand. The testing program occurred over the course of 12 months from February 2018 to February 2019. Table 4.1 shows the test number, date performed and average bladder pressure for all tests in this testing program. Tests were conducted with a goal average vertical effective stress of approximately 10 psi, 20 psi and 30 psi for each respective soil condition.

Two tests were conducted without a casing. In these tests, soil in the chamber was in direct contact with the side of the model drilled shaft. The remaining seven tests were conducted with a steel casing. In the cased tests, soil was only in contact with the tip of the foundation. In the tests without a casing, the same procedure outlined in Chapter 3 was utilized.

Table 4.1 Test number, data and average bladder pressure for all tests

Test No.	Date	Average Bladder Pressure (psi)
1	2/20/18	10.1
2	3/20/18	20.5
3	9/13/18	30.2
4	9/25/18	10.4
5	10/11/18	20.5
6	10/24/18	30.2
7	11/15/18	10.3
8	1/30/19	18.8
9	2/4/19	30.6

4.2 Mobilized Side Friction of Uncased Load Tests

O'Neil and Reese (1999) proposed a method for determining the mobilized side friction for drilled shaft foundations in cohesionless soil. Figure 4.1 details the relationship. The method relates the shaft settlement, w_b divided by the base diameter, D, to the ratio of the developed side resistance, f_s to the ultimate side resistance, $f_{s,ult}$.

This method was used to estimate the contribution that side resistance had on the ultimate load from the load cell for test 1 and 2 in this testing program. After determining the magnitude of the side resistance the contribution was subtracted from force read by the load cell. This was done to ensure all tests in this program would be comparing base resistance. The loose sand tests performed at a target bladder pressure of 10 psi and 20 psi were both uncased and the load cell forces for each test were adjusted using this method.

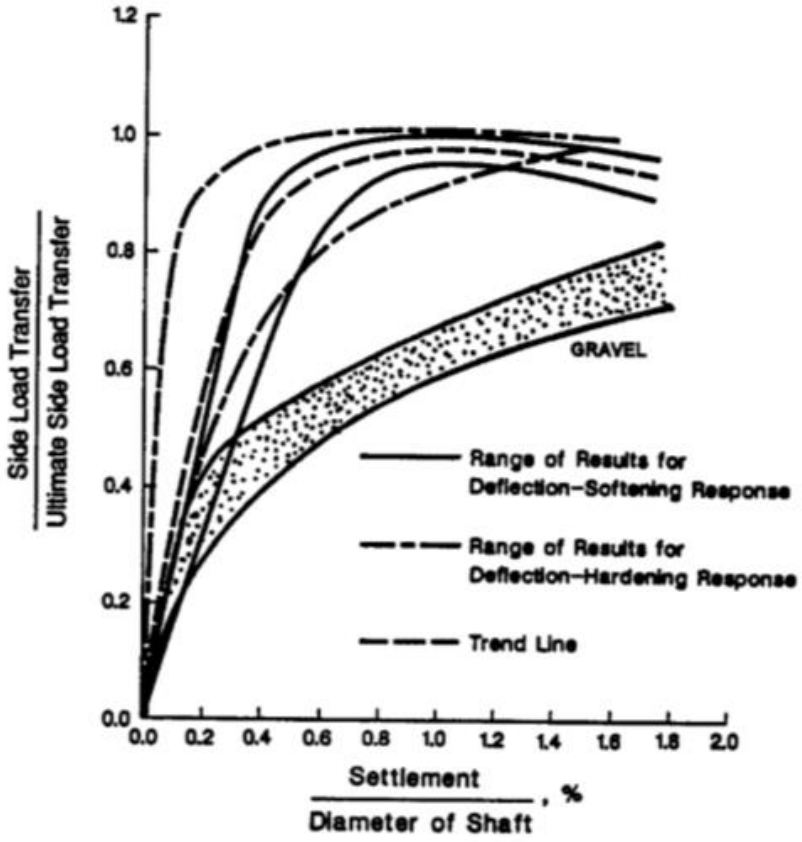

Figure 4.1 Normalized side load transfer for drilled shaft foundations in cohesionless soil proposed by Reese and O'Neil (1999)

4.3 Tests in Loose Poorly Graded Sand

Three axial load-displacement tests were performed in loose poorly graded sand with a range of overburden pressure from 10 psi to 30 psi. The results of the tests, including a summary of the soil conditions, average vertical effective stress over the course of the test, and a plot of the axial load versus displacement are presented. Tests performed in a loose configuration were achieved by dropping the soil from a dump bucket through a pluviation device. The device is explained in more detail in Section 3.6.1. The pluviation device is an attachment with multiple levels of sieves. As soil enters the device it is scattered upon impact with the sieves. The

resulting soil has a more uniform deposition compared to dropping directly from the dump bucket.

4.3.1 Test 1 – Loose Poorly Graded Sand with 10psi Overburden Stress

Test 1 was performed in loose poorly graded sand with a goal overburden pressure of 10 psi. The test was performed in the experimental apparatus without a casing. The soil was placed in a loose condition using a pluviation device attached to the underside of the dump bucket. Table 4.2 Summarizes the soil conditions for Test 1. Figure 4.2 shows the vertical overburden stress versus time for Test 1. The average vertical effective stress was 10.1 psi.

Table 4.2 Summary of soil conditions for Test 1

Test No.	Soil Type	Dry Unit Weight, γ_{dry} (pcf)	Average Water Content (%)	Relative Density, D_r (%)	Soil Density	Average Vertical Effective Stress, σ'_v (psf)	Casing used
1	SP	87.4	0.3	12.1	Loose	1651	N

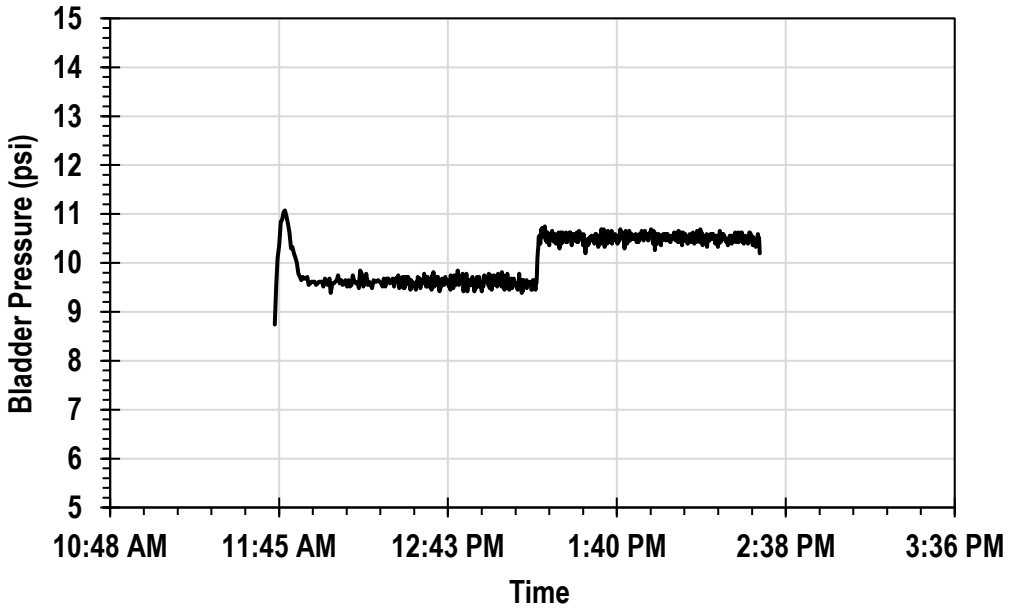

Figure 4.2 Overburden stress versus time during Test 1

The axial load-settlement curve for Test 1 is shown in Figure 4.3. The model drilled shaft foundation was loaded to a maximum axial load of 40.8 kips with four load-unload cycles at 5.1 kips, 10.2 kips, 17.4 kips and 29.9 kips. A fifth load-unload-reload cycle was attempted with a goal load of 45 kips. Due to one of the rubber tubes in the bladder system bursting the test was concluded before reaching the goal load. The LVDT measuring displacement on the east side of the top of the model foundation was used to measure displacement. The model drilled shaft foundation displaced a total of 1.81 inches.

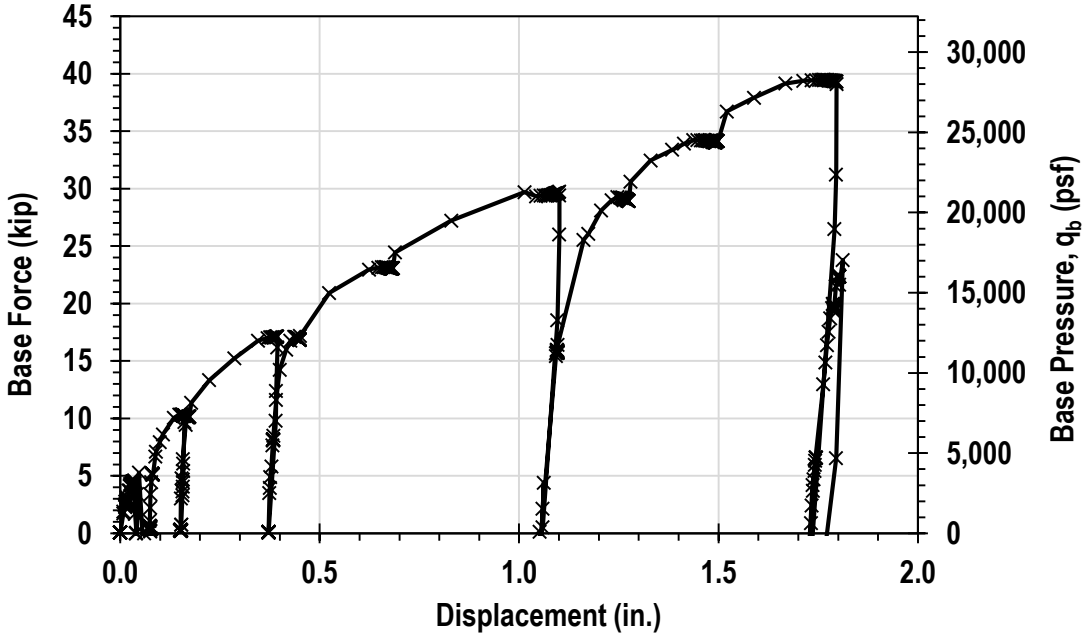

Figure 4.3 Axial load-displacement relationship for loose poorly graded sand with 10 psi overburden stress

4.3.2 Test 2 – Loose Poorly Graded Sand with 20psi Overburden Stress

Test 2 was performed in in loose poorly graded sand with a goal overburden pressure of 20 psi. The test was performed in the experimental apparatus without a casing. The soil was placed in a loose condition using a pluviation device attached to the underside of the dump bucket. Table 4.3 Summarizes the soil conditions for Test 2. Figure 4.4 shows the vertical overburden stress versus time for Test 2. The average vertical effective stress during the test was 20.5 psi.

Table 4.3 Summary of soil conditions for Test 2

Test No.	Soil Type	Dry Unit Weight, γ_{dry} (pcf)	Average Water Content (%)	Relative Density, D_r (%)	Soil Density	Average Vertical Effective Stress, σ'_v (psf)	Casing used
2	SP	95.6	0.3	24.9	Loose	3167	N

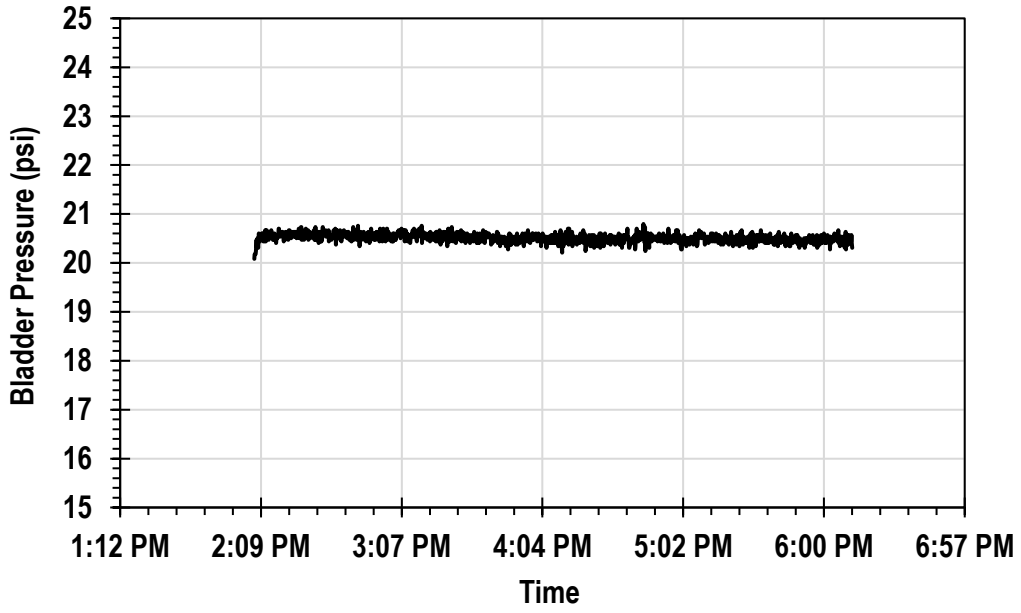

Figure 4.4 Overburden stress versus time during Test 2

The axial load-settlement curve for Test 2 is shown in Figure 4.5. The model drilled shaft foundation was loaded to a maximum axial load of 46.0 kips with five load-unload cycles at 6.5 kips, 16.5 kips, 25.1 kips, 33.9 kips and 39.4 kips. The LVDT measuring displacement on the east side of the top of the model foundation was used to measure displacement. The model drilled shaft foundation displaced a total of 2.83 inches.

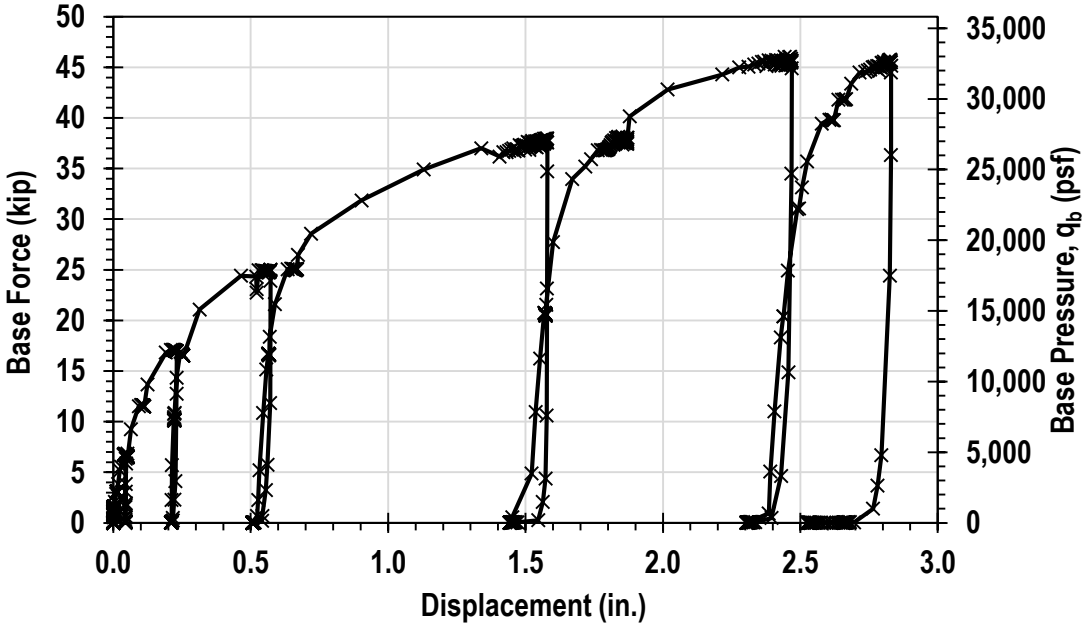

Figure 4.5 Axial load-displacement relationship for loose poorly graded sand with 20 psi overburden stress

4.3.3 Test 3 – Loose Poorly Graded Sand with 30psi Overburden Stress

Test 3 was performed in loose poorly graded sand with a goal overburden pressure of 30 psi. The test utilized a casing to reduce the influence of side resistance on the foundation. The casing is described in more detail in Section 3.3.2. The soil was placed in a loose condition using a pluviation device attached to the underside of the dump bucket. Table 4.4 Summarizes the soil conditions for Test 2. Figure 4.6 shows the vertical overburden stress versus time for Test 2. The average vertical effective stress during the test was 30.2 psi.

Table 4.4 Summary of soil conditions for Test 3

Test No.	Soil Type	Dry Unit Weight, γ_{dry} (pcf)	Average Water Content (%)	Relative Density, D_r (%)	Soil Density	Average Vertical Effective Stress, σ'_v (psf)	Casing used
3	SP	92.5	0.3	6.2	Loose	4557	Y

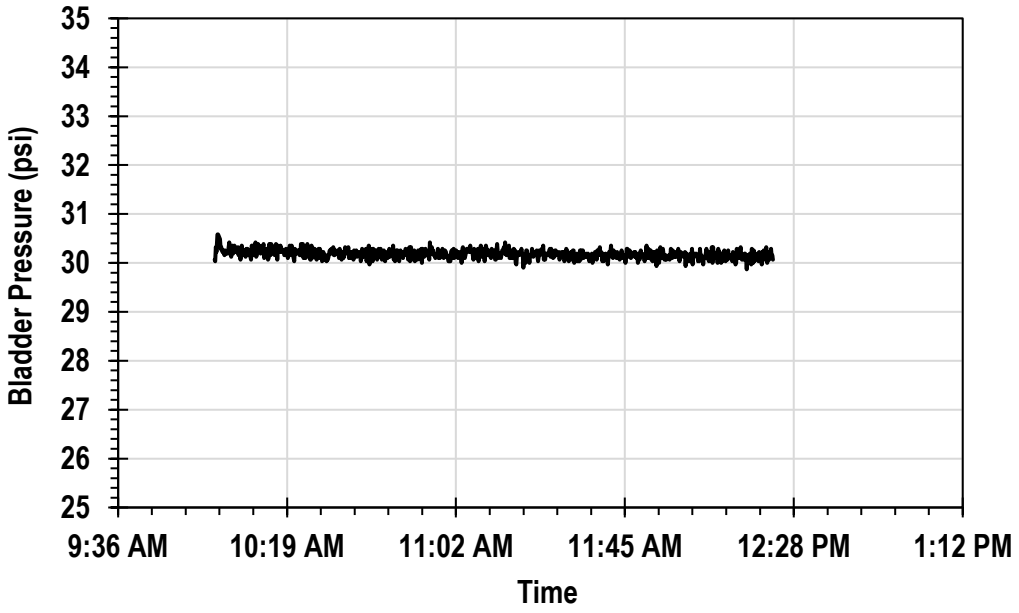

Figure 4.6 Overburden stress versus time during Test 3

The axial load-settlement curve for this test is shown in Figure 4.7. The model drilled shaft foundation was loaded to a maximum axial load of 36.7 kips with three load-unload cycles at 3.0 kips, 11.5 kips and 21.4 kips. The LVDT measuring displacement on the north side of the top of the model foundation was used to measure displacement. The model drilled shaft foundation displaced a total of 1.65 inches. It is important to note that the 11.5 kips axial load was removed all at once instead of in increments during the second load-unload-reload cycle on accident.

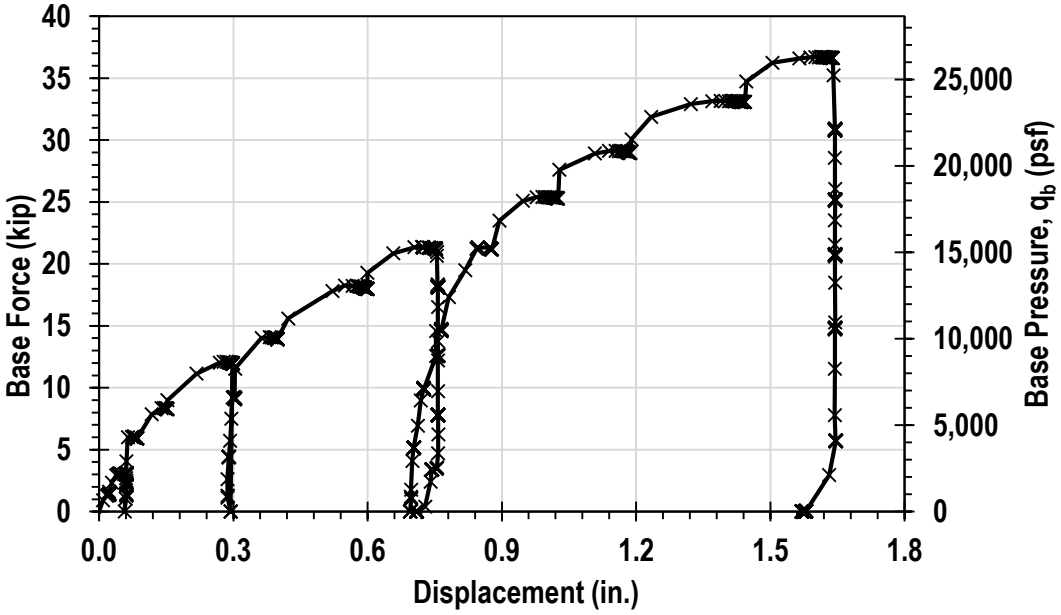

Figure 4.7 Axial load-displacement relationship for loose poorly graded sand with 30 psi overburden stress

4.4 Tests in Loose Poorly Graded Sand

Three axial load-displacement tests were performed in dense poorly graded sand with a range of overburden pressure from 10 psi to 30 psi. In order to achieve a dense configuration, the soil was placed in lifts approximately six inches high and compacted using a 10-inch by 10-inch flat plate tamper. The compaction method is described in Section 3.6.1. The results of the tests, including a summary of the soil conditions, average vertical effective stress over the course of the test, and a plot of the axial load versus displacement are presented.

4.4.1 Test 4 – Dense Poorly Graded Sand with 10psi Overburden Stress

Test 4 was performed in in dense poorly graded sand with a goal overburden pressure of 10 psi. The test was performed in the experimental apparatus with a casing. The soil was placed in a dense configuration using a flat plate tamper. Table 4.5 Summarizes the soil conditions for

Test 4. Figure 4.8 shows the vertical overburden stress versus time for Test 4. The average vertical effective stress during the test was 10.4 psi.

Table 4.5 Summary of soil conditions for Test 4

Test No.	Soil Type	Dry Unit Weight, γ_{dry} (pcf)	Average Water Content (%)	Relative Density, D_r (%)	Soil Density	Average Vertical Effective Stress, σ'_v (psf)	Casing used
4	SP	104.2	0.3	76.9	Dense	1732	Y

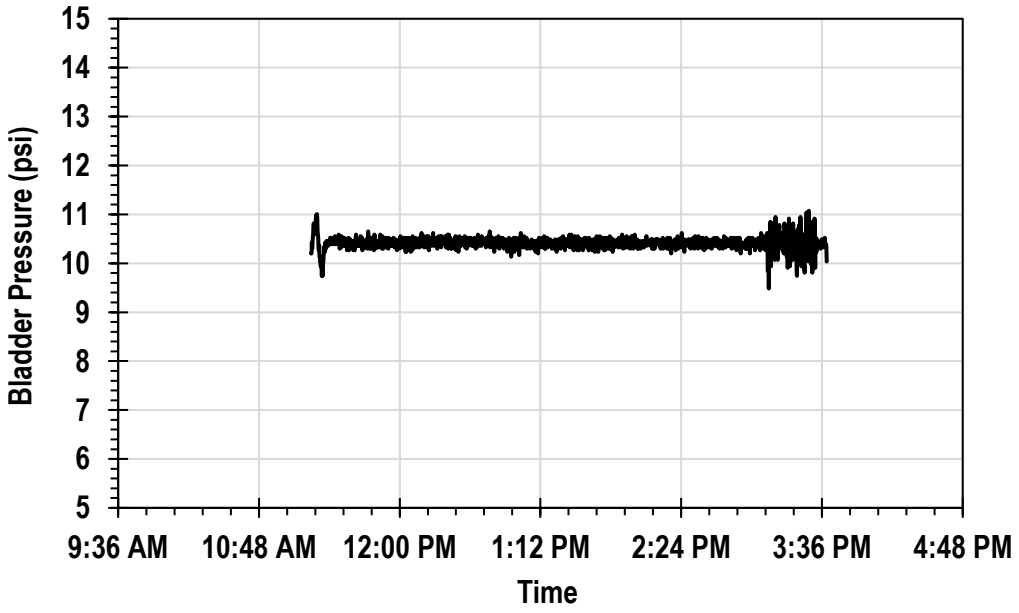

Figure 4.8 Overburden stress versus time during Test 4

The axial load-settlement curve for this test is shown in Figure 4.9. The model drilled shaft foundation was loaded to a maximum axial load of 70.4 kips with six load-unload-reload cycles at 3.3 kips, 8.3 kips, 11.1 kips, 19.7 kips, 34.1 kips and 50.9 kips. The LVDT measuring displacement on the south side of the top of the model foundation was used to measure displacement. The model drilled shaft foundation displaced a total of 0.73 inches.

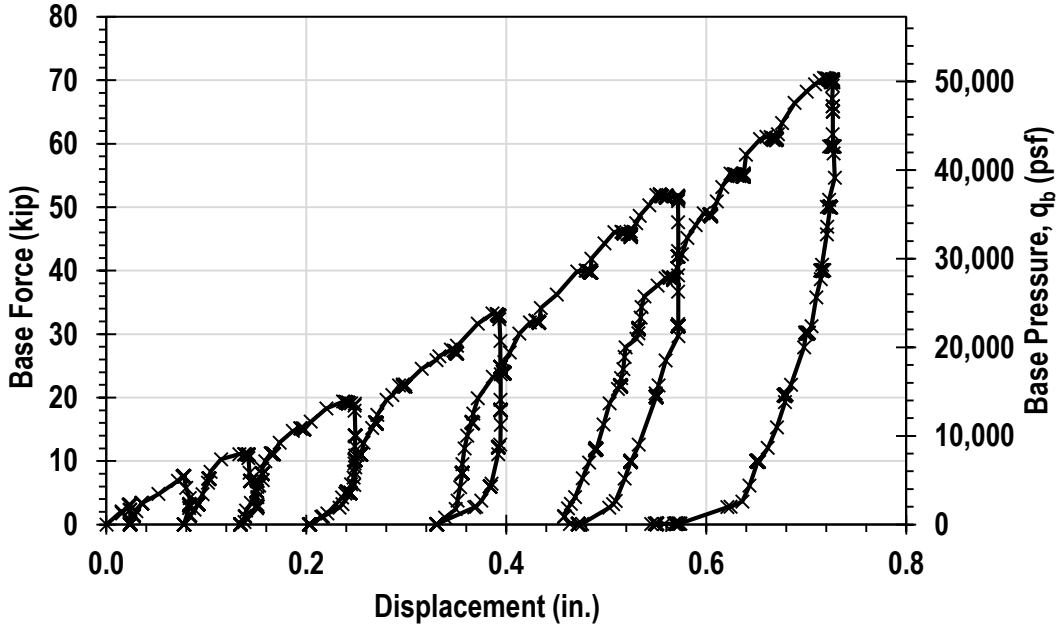

Figure 4.9 Axial load-displacement relationship for dense poorly graded sand with 10 psi overburden stress

This test exhibited a different load-settlement behavior compared to what was observed in the tests with the same soil in a loose configuration. It is important to note magnitude of displacements in the dense configuration were significantly smaller than those observed in the loose configuration. Larger loads were also required to reach a fraction of the displacement seen at smaller loads in the loose configuration.

The displacements of the north top of foundation and south top of foundation LVDTs varied largely compared to the total magnitude of displacement. Figure 4.10 shows the axial load-displacement behavior from two LVDTs placed at the top of the foundation. The varability in displacements indicates that the foundation was rotating during loading. During examination of the data, the rotation was relatively small near the beginning of the test. As the test proceeded, the degree of variation in the data increased. The excessive rotation could have also been caused by many factors. The difference could have been caused by an anomaly in the soil profile

directly below the model foundation. The displacement measurement from the LVDT resting on the south side of the top of the model foundation was used. This data was most comparable to hand measurements from a manual dial gage. The results from the north LVDT also more closely align with data from other tests performed in similar soil configurations.

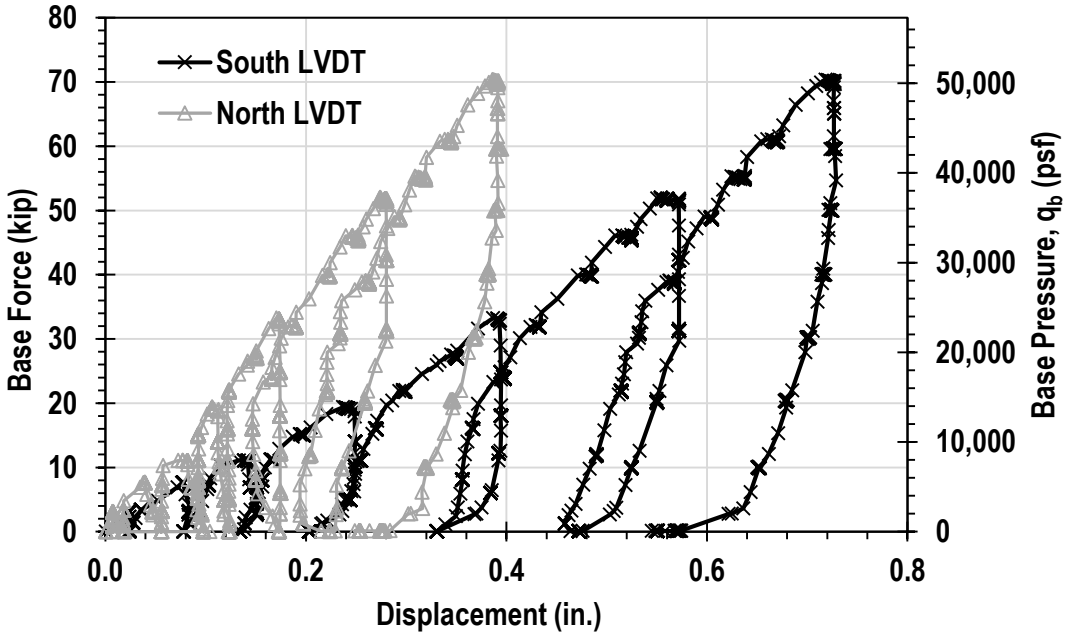

Figure 4.10 Axial load-displacement result from two LVDTs during Test 4

4.4.2 Test 5 – Dense Poorly Graded Sand with 20psi Overburden Stress

Test 5 was performed in in dense poorly graded sand with a goal overburden pressure of 20 psi. The test was performed in the experimental apparatus with a casing. The soil was placed in a dense configuration using a flat plate tamper. Table 4.6 Summarizes the soil conditions for Test 4. Figure 4.11 shows the vertical overburden stress versus time for Test 5. The average vertical effective stress during the test was 20.5 psi.

Table 4.6 Summary of soil conditions for Test 5

Test No.	Soil Type	Dry Unit Weight, γ_{dry} (pcf)	Average Water Content (%)	Relative Density, D_r (%)	Soil Density	Average Vertical Effective Stress, σ'_v (psf)	Casing used
5	SP	105.7	0.3	86.0	Dense	3190	Y

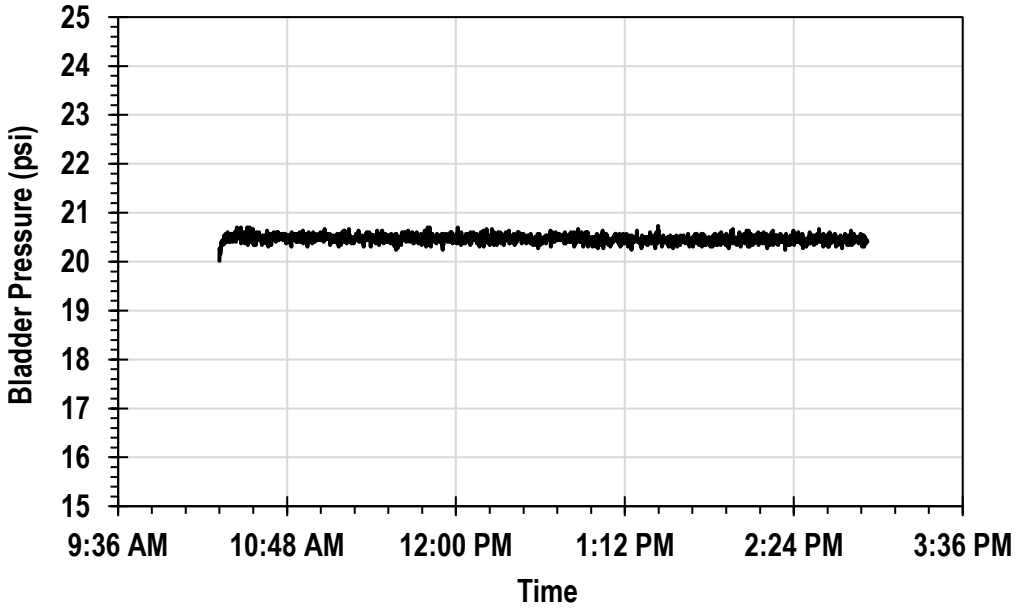

Figure 4.11 Overburden stress versus time during Test 5

The axial load-settlement curve for this test is shown in Figure 4.12. The model drilled shaft foundation was loaded to a maximum axial load of 70.3 kips with seven load-unload-reload cycles at 3.1 kips, 7.1 kips, 12.9 kips, 19.9 kips, 32.8 kips, 51.8 kips and 68.8 kips. The LVDT measuring displacement on the south side of the top of the model foundation was used to measure displacement. The model drilled shaft foundation settled a total of 0.73 inches.

This test experienced only one issue where the west LVDT measuring displacement from the base of the foundation was not translating freely. Data from the LVDT was omitted from this testing program.

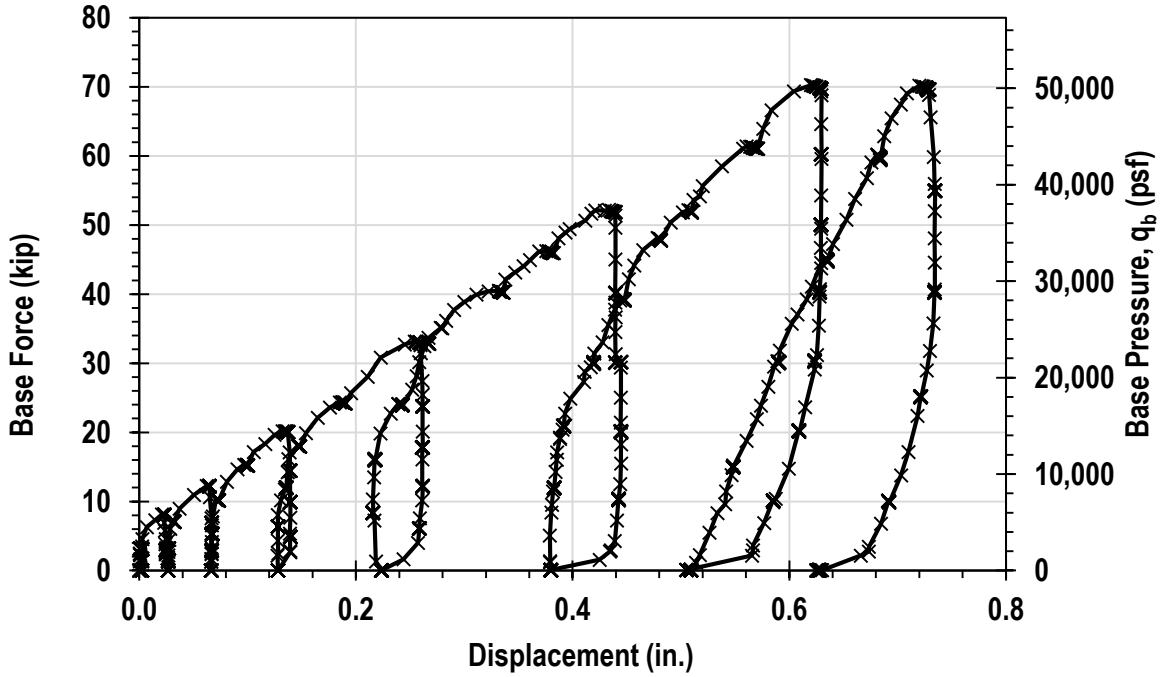

Figure 4.12 Axial load-displacement relationship for dense poorly graded sand with 20 psi overburden stress

4.4.3 Test 6 – Dense Poorly Graded Sand with 30psi Overburden Stress

Test 6 was performed in in dense poorly graded sand with a goal overburden pressure of 30 psi. The test was performed in the experimental apparatus with a casing. The soil was placed in a dense configuration using a flat plate tamper. Table 4.7 Summarizes the soil conditions for Test 6. Figure 4.13 shows the vertical overburden stress versus time for Test 6. The average vertical effective stress during the test was 30.2 psi.

Table 4.7 Summary of soil conditions for Test 6

Test No.	Soil Type	Dry Unit Weight, γ_{dry} (pcf)	Average Water Content (%)	Relative Density, D_r (%)	Soil Density	Average Vertical Effective Stress, σ'_v (psf)	Casing used
6	SP	106	0.3	87.8	Dense	4587	Y

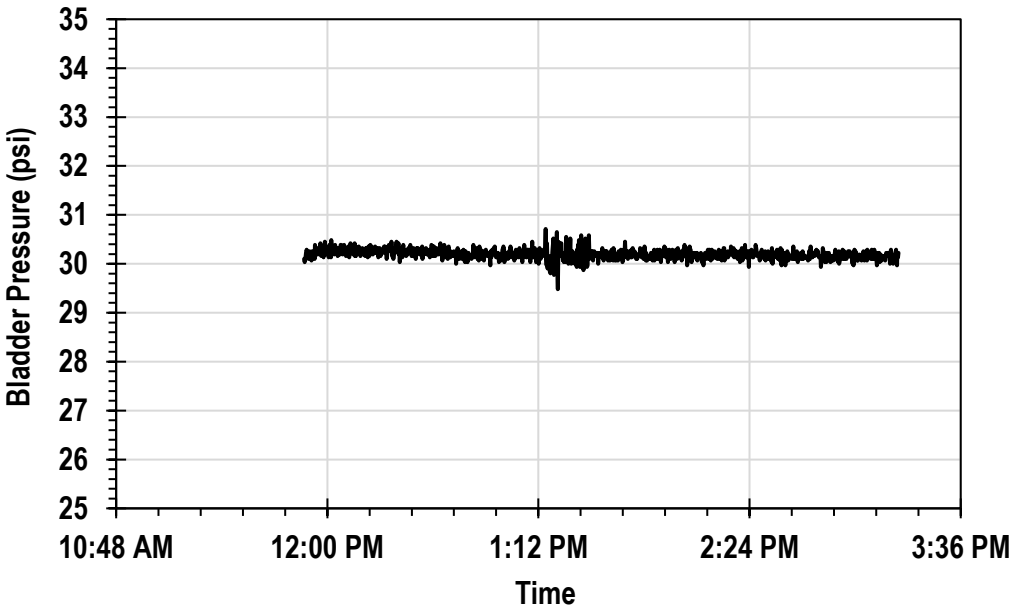

Figure 4.13 Overburden stress versus time during Test 6

The axial load-settlement curve for this test is shown in Figure 4.14. The model drilled shaft foundation was loaded to a maximum axial load of 61.7 kips with seven load-unload-reload cycles at 3.4 kips, 7.7 kips, 12.2 kips, 20.0 kips, 35.8 kips, 48.1 kips and 59.8 kips. The LVDT measuring displacement on the north side of the top of the model foundation was used to measure displacement. The model drilled shaft foundation settled a total of 0.43 inches.

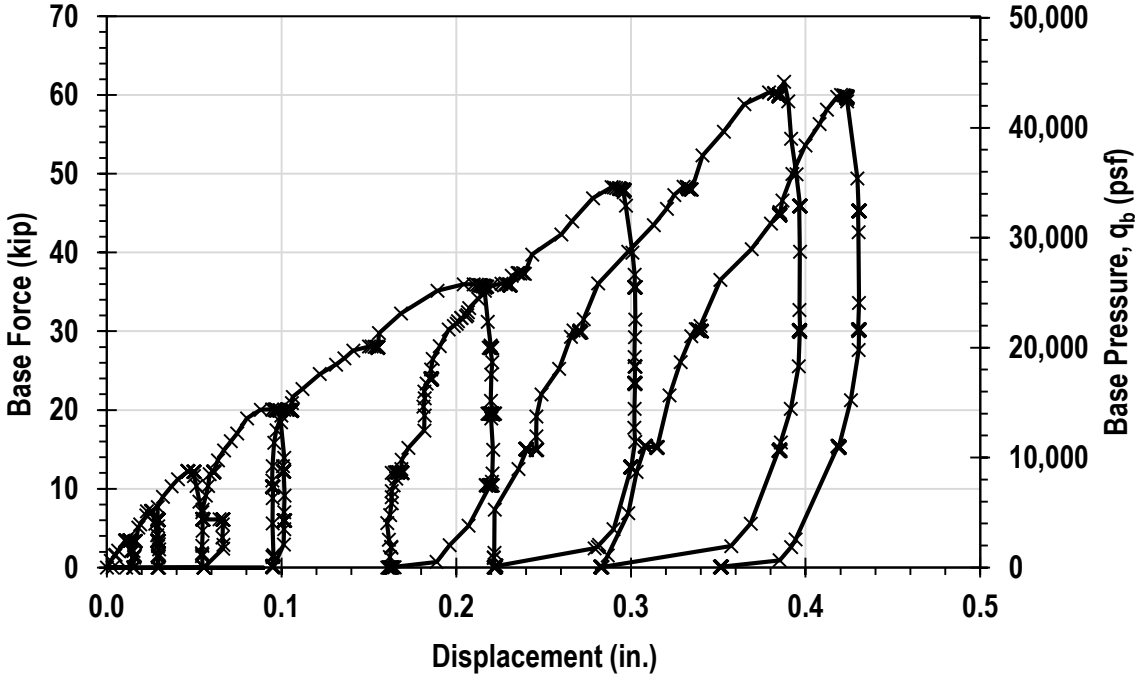

Figure 4.14 Axial load-displacement relationship for dense poorly graded sand with 30 psi overburden stress

4.5 Tests in Compacted Silty Sand

Three axial load-displacement tests were performed in compacted silty sand with a range of overburden pressure from 10 psi to 30 psi. In order to achieve a dense configuration, the soil was placed in six-inch high lifts and compacted using a 10-inch by 10-inch flat plate tamper. The compaction method is described in Section 3.6.1 Experimental Setup. The results of the tests, including a summary of the soil conditions, average vertical effective stress over the course of the test, and a plot of the axial load versus displacement are presented.

4.5.1 Test 7 – Compacted Silty Sand with 10psi Overburden Stress

Test 7 was performed in in compacted silty sand with a goal overburden pressure of 10 psi. The test was performed in the experimental apparatus with a casing. The soil was compacted using a flat plate tamper. Table 4.8 Summarizes the soil conditions for Test 7. Figure 4.15 shows

the vertical overburden stress versus time for Test 6. The average vertical effective stress during the test was 10.3 psi.

Table 4.8 Summary of soil conditions for Test 7

Test No.	Soil Type	Dry Unit Weight, γ_{dry} (pcf)	Average Water Content (%)	Relative Density, D_r (%)	Soil Density	Average Vertical Effective Stress, σ'_v (psf)	Casing used
7	SM	123.2	11.7	n/a	Dense	1760	Y

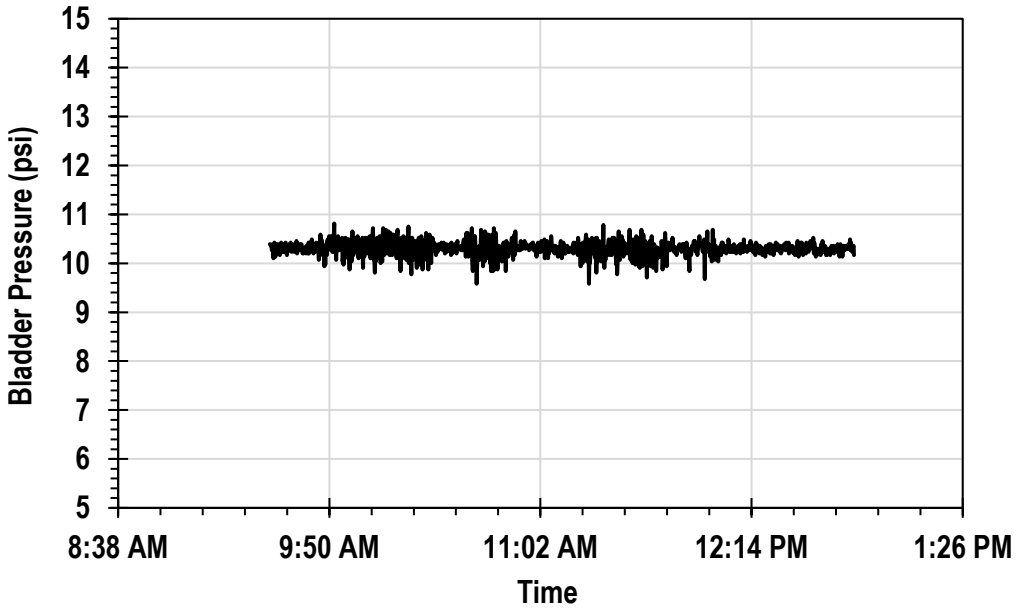

Figure 4.15 Overburden stress versus time during Test 7

The axial load-settlement curve for this test is shown in Figure 4.16 The model drilled shaft foundation was loaded to a maximum axial load of 15.9 kips with four load-unload-reload cycles at 3.5 kips, 6.6 kips, 9.9 kips and 12.5 kips. The LVDT measuring displacement on the south side of the top of the model foundation was used to measure displacement. The model drilled shaft foundation settled a total of 2.98 inches.

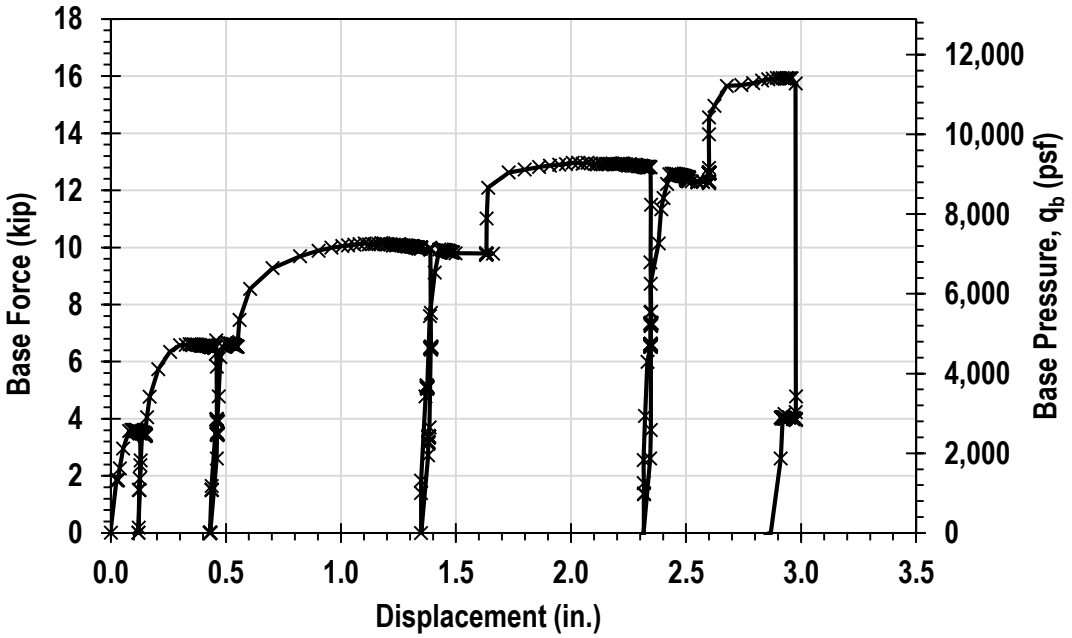

Figure 4.16 Axial load-displacement relationship for compacted silty sand with 10 psi overburden stress

4.5.2 Test 8 – Compacted Silty Sand with 20psi Overburden Stress

Test 8 was performed in in compacted silty sand with a goal overburden pressure of 20 psi. The test was performed in the experimental apparatus with a casing. The soil was compacted using a flat plate tamper. Table 4.9 Summarizes the soil conditions for Test 8. Figure 4.17 shows the vertical overburden stress versus time for Test 8. The average vertical effective stress during the test was 18.8 psi.

Table 4.9 Summary of soil conditions for Test 8

Test No.	Soil Type	Dry Unit Weight, γ_{dry} (pcf)	Average Water Content (%)	Relative Density, D_r (%)	Soil Density	Average Vertical Effective Stress, σ'_v (psf)	Casing used
8	SM	122.4	10.8	n/a	Dense	2983	Y

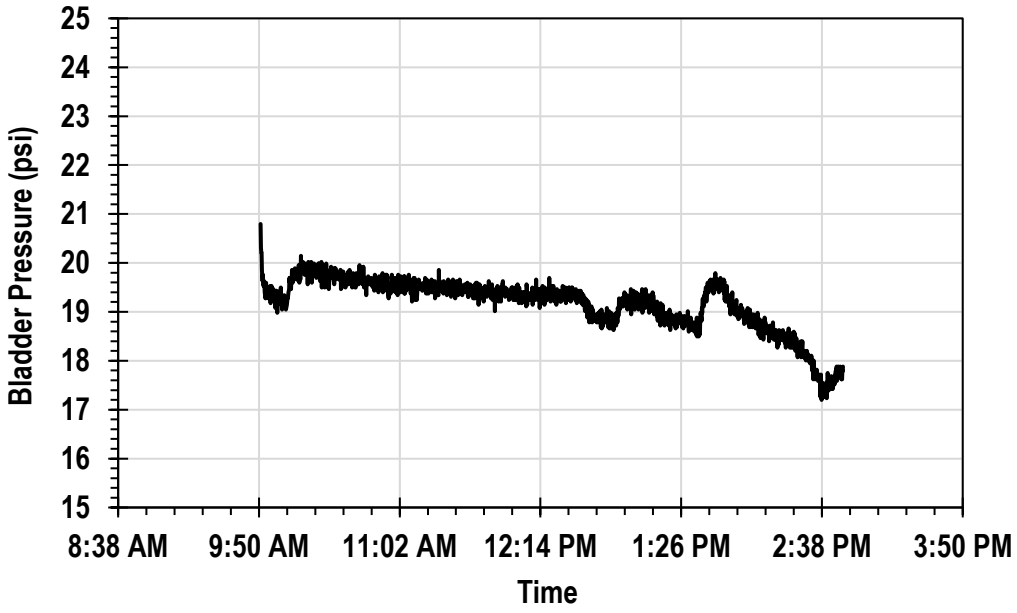

Figure 4.17 Overburden stress versus time during Test 8

The axial load-settlement curve for this test is shown in Figure 4.18. The model drilled shaft foundation was loaded to a maximum axial load of 15.3 kips with four load-unload-reload cycles at 3.2 kips, 6.1 kips, 9.2 kips and 12.1 kips. The LVDT measuring displacement on the north side of the top of the model foundation was used to measure displacement. The model drilled shaft foundation settled a total of 2.88 inches.

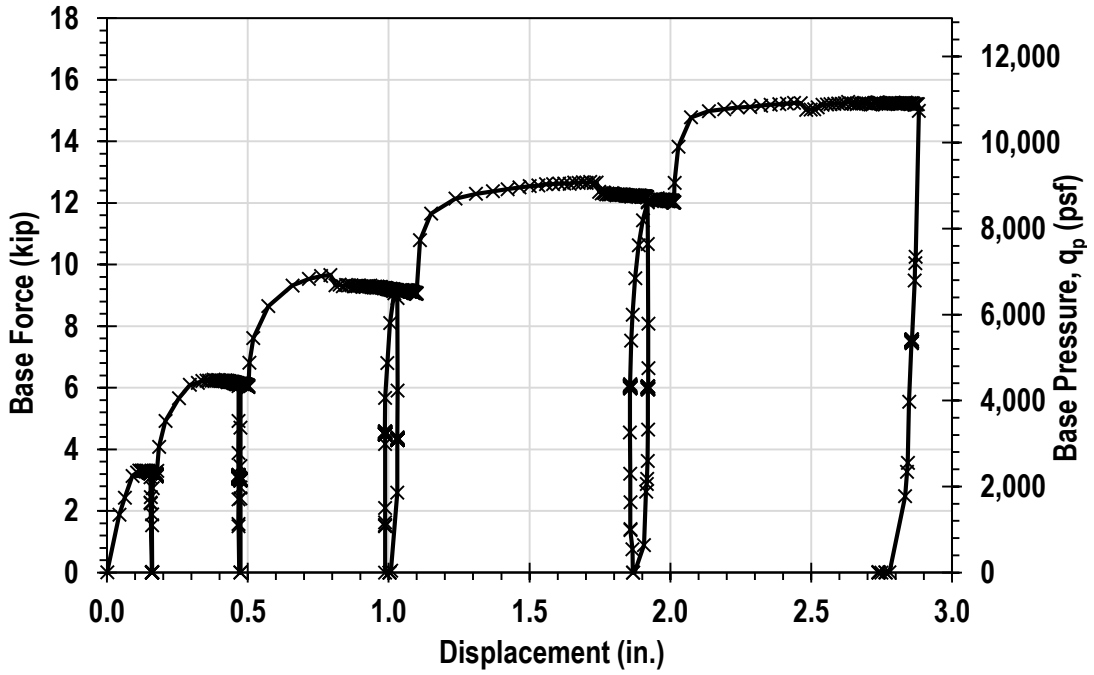

Figure 4.18 Axial load-displacement relationship for compacted silty sand with 20 psi overburden stress

4.5.3 Test 9 – Compacted Silty Sand with 30psi Overburden Stress

Test 9 was performed in in compacted silty sand with a goal overburden pressure of 30 psi. The test was performed in the experimental apparatus with a casing. The soil was compacted using a flat plate tamper. Table 4.10 Summarizes the soil conditions for Test 9. Figure 4.19 shows the vertical overburden stress versus time for Test 9. The average vertical effective stress during the test was 30.6 psi.

Table 4.10 Summary of soil conditions for Test 9

Test No.	Soil Type	Dry Unit Weight, γ_{dry} (pcf)	Average Water Content (%)	Relative Density, D_r (%)	Soil Density	Average Vertical Effective Stress, σ'_v (psf)	Casing used
9	SM	119.5	10.5	n/a	Dense	4675	Y

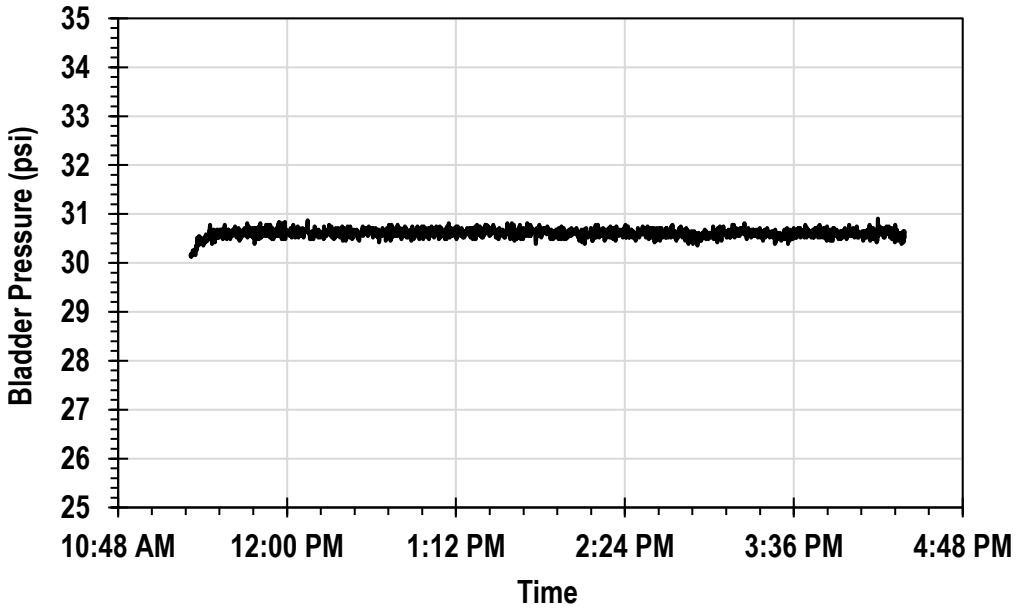

Figure 4.19 Overburden stress versus time during Test 9

The axial load-settlement curve for this test is shown in Figure 4.20. The model drilled shaft foundation was loaded to a maximum axial load of 12.2 kips with four load-unload-reload cycles at 3.3 kips, 6.1 kips, 9.3 kips and 12.2 kips. The LVDT measuring displacement on the north side of the top of the model foundation was used to measure displacement. The model drilled shaft foundation settled a total of 1.21 inches.

An attempt was made to increase the axial load to a goal load of 15 kips but was unsuccessful. The foundation began to rotate, and any further displacement caused by increasing the load would have caused the foundation to contact the lid of the experimental apparatus.

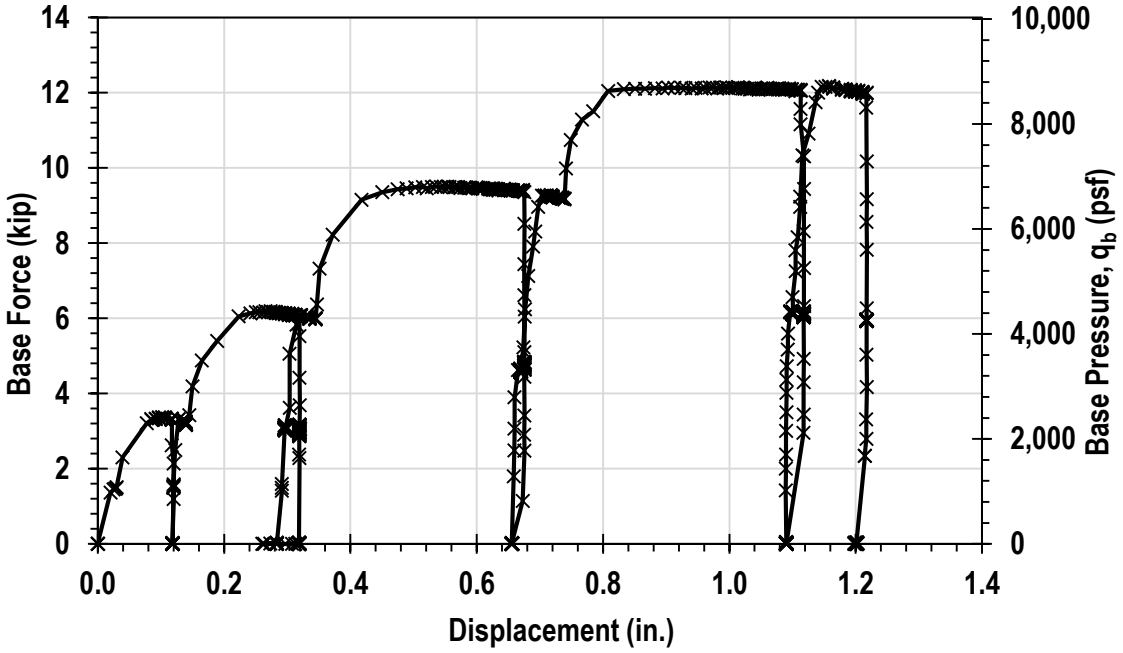

Figure 4.20 Axial load-displacement relationship for compacted silty sand with 30 psi overburden stress

4.6 Summary

In this chapter the results of the testing program were presented. The results were detailed on a test-by-test basis divided into groups based on soil configuration. The results from each individual test are further broken down based on the overburden pressure applied. Results presented for each test include details about specific soil conditions and any issues that arose during testing that would be pertinent to subsequent analysis of the data. The load-unload-reload method detailed in the testing procedure section of Chapter 3 was utilized for all tests presented.

Chapter 5 Analysis

The data presented in Chapter 4 were analyzed in order to determine how the soil stiffness changed during the reloading portion of a load-unload-reload cycle with displacement. Three different soil conditions were examined utilizing a model drilled shaft foundation. In this chapter, the reload stiffness is examined based on soil configuration and displacement. A relationship between the reload stiffness and displacement is developed based on the experimental measurements presented in Chapter 4. The values are compared to the results of a field load test found in literature.

5.1 Analysis Procedure

Results of the axial load-displacement tests performed in three different soil conditions were analyzed in order to develop a relationship between reload stiffness and displacement. After an estimate of the base load was determined, the reload stiffness was determined by fitting a linear line through points on the reload portion of the axial load-displacement plot for each test. Figure 5.1 shows linear lines used to determine the reload stiffness were fit in a typical test. The slope of the lines in color were calculated to determine the reload stiffness. The reload stiffness values were plotted versus the displacement at the end of reloading. A total of nine tests were used in this analysis.

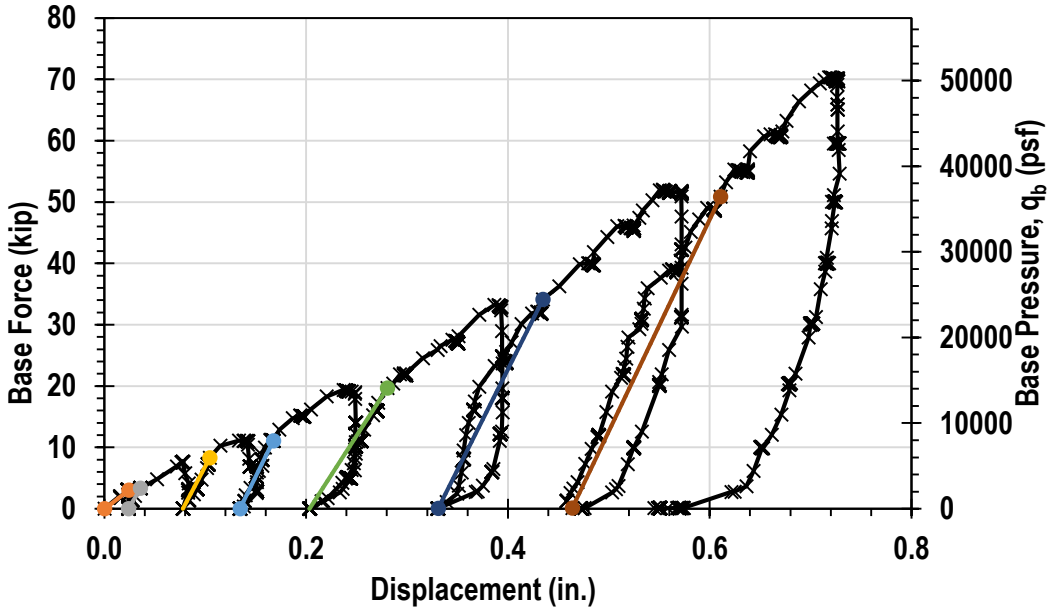

Figure 5.1 A typical test showing linear lines fit to the reload portion of a plot of axial load versus displacement

5.3 Reload Stiffness in Individual Tests

The reload stiffness was determined from axial force versus displacement plots for each test. The number of reload stiffness values collected varied depending on the number of load-unload-reload cycles performed in each test. The reload stiffness from each soil configuration was plotted together.

5.3.1 Loose Sand

Figure 5.2 shows the reload stiffness from tests performed in loose poorly graded clean sand versus displacement. The overburden stress applied are detailed with different symbols. The reload stiffness was initially large at low displacements and decreased toward a constant value as displacement increased. An exponential function was fit to the data.

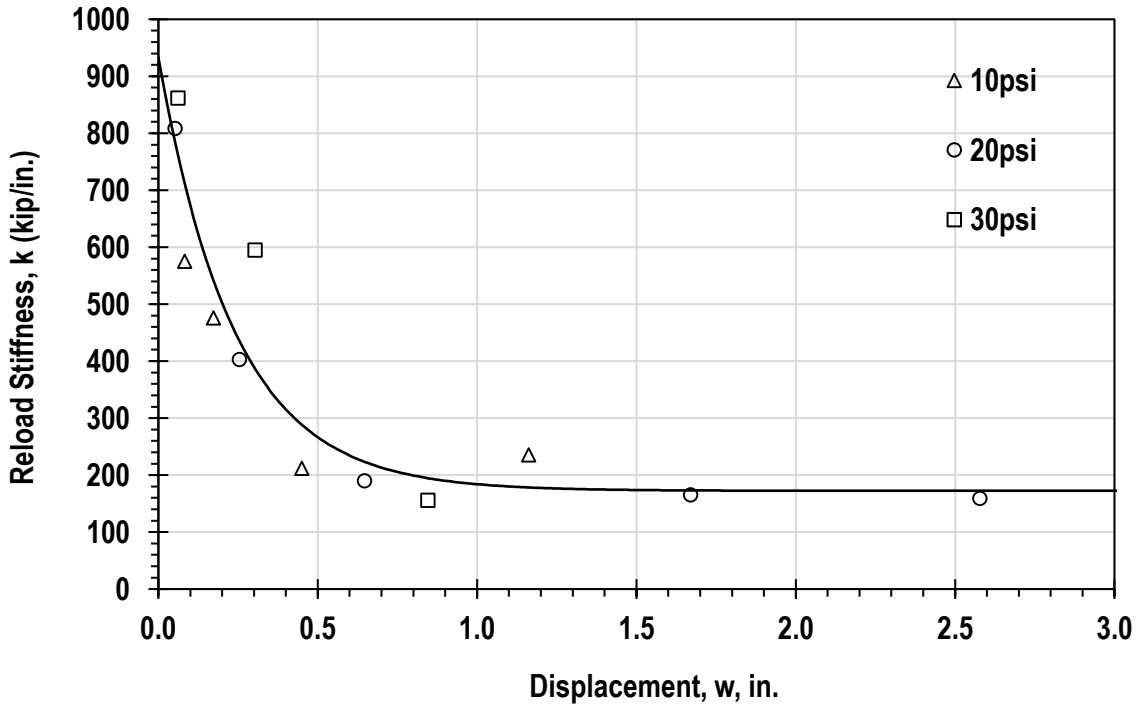

Figure 5.2 Reload stiffness, k (kip/in.) versus displacement, w (in.) for tests in loose sand

5.3.2 Dense Sand

Figure 5.3 shows the reload stiffness from tests performed in dense poorly graded clean sand versus displacement. The overburden stress applied are detailed with different symbols. The reload stiffness was initially large at low displacements and decreased as displacement increased. Figure 5.3 also shows an exponential function fit to the reload stiffness from tests in dense sand versus displacement. Two exponential functions were fit to tests performed in the dense sand configuration. Fit 1 was a fit through the data collected for dense sand in this testing program. The fit suggested that the reload stiffness would begin to reach a constant value in the range of 362 kip/in. The second fit was fit through all tests performed in poorly graded clean sand. Figure 5.4 shows the second fit through data from loose and dense configurations of the poorly graded clean sand. The load-deformation response of the model foundation in dense sand was not

examined at large displacements as observed in tests with clean sand in the loose configuration. Fit 2 was shows that at larger displacements the reload stiffness will likely reach the same constant value observed in tests in the loose clean sand configuration.

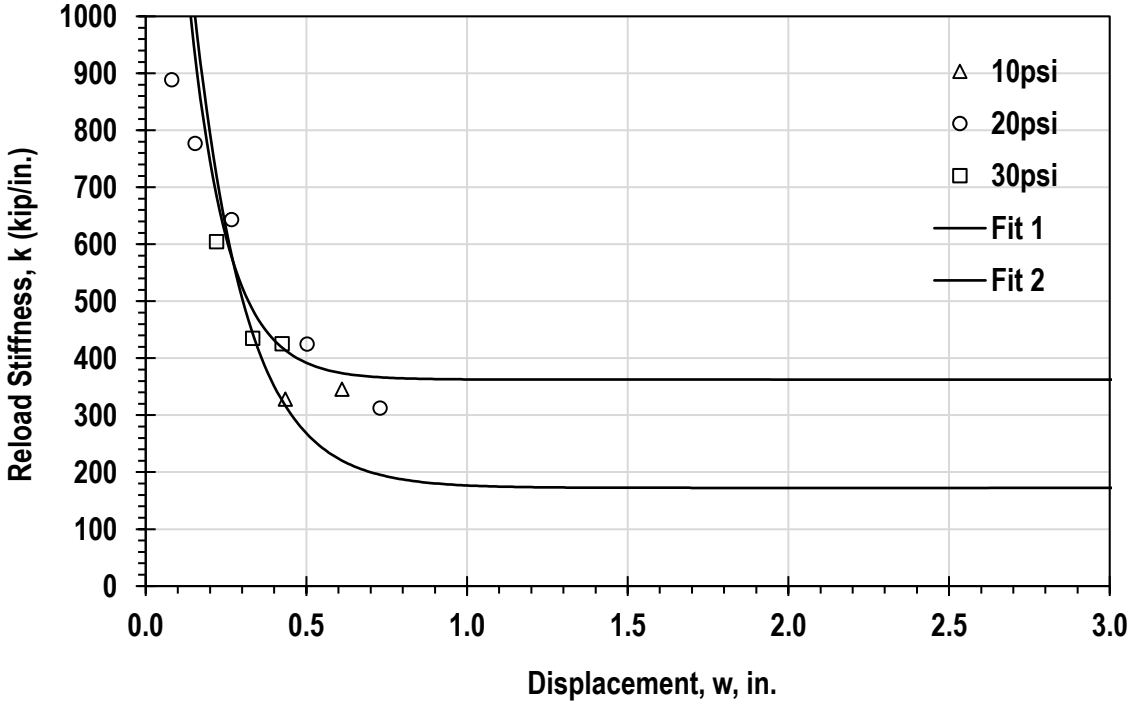

Figure 5.3 Reload stiffness, k (kip/in.) versus displacement, *w* (in.) for tests in dense sand

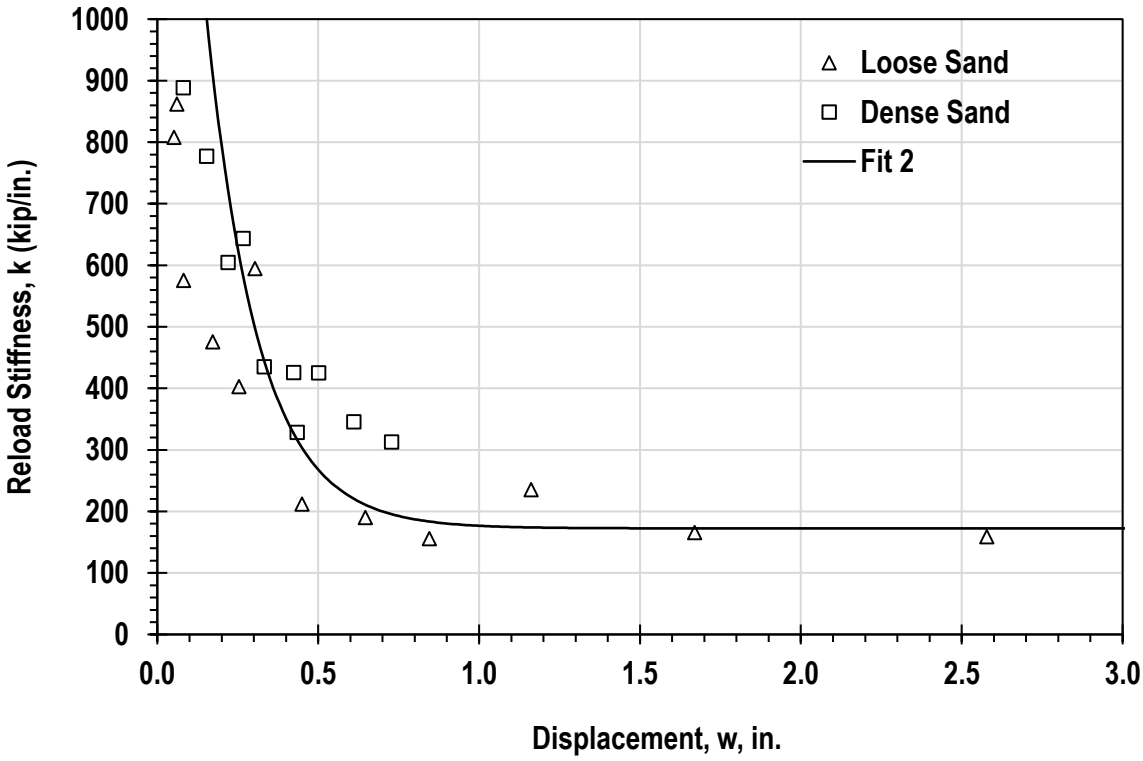

Figure 5.4 Reload stiffness, k (kip/in.) versus displacement, *w* (in.) for tests in poorly graded clean sand

5.3.3 Silty Sand

Figure 5.5 shows the reload stiffness from tests performed in compacted silty sand versus displacement. The overburden stress applied are detailed with different symbols. The reload stiffness remained constant and the data showed a different trend compared to the clean sand tests. The reload stiffness in tests with silty sand were relatively close together and did not follow the same trend as tests in clean sand.

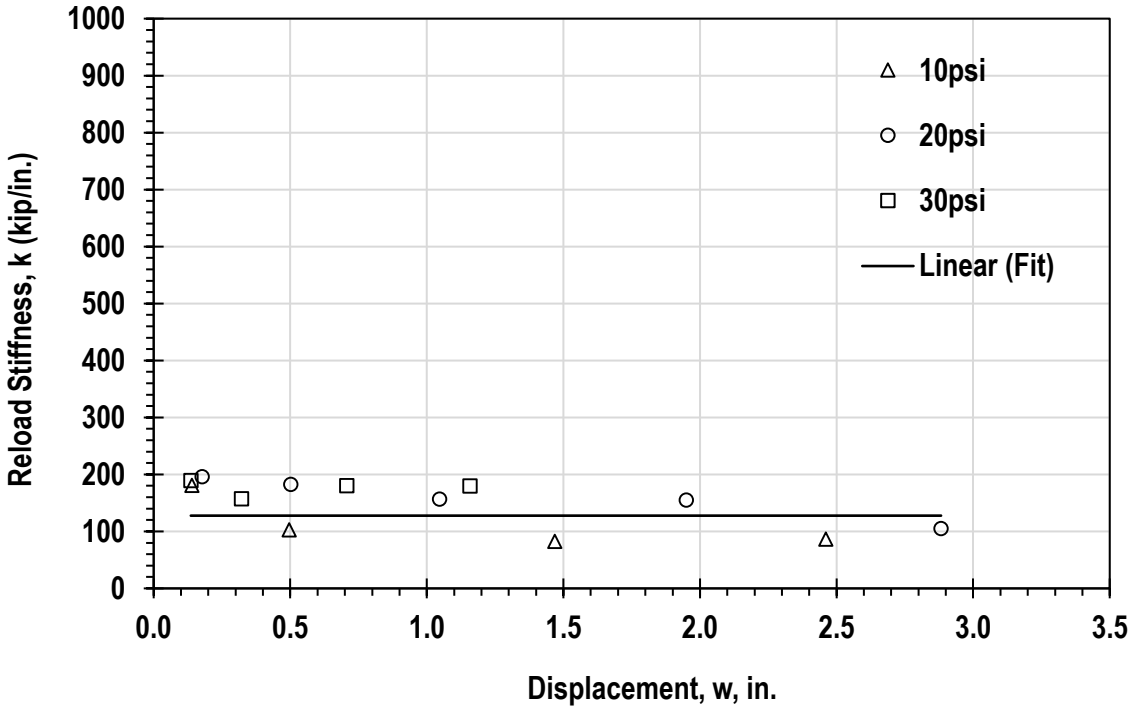

Figure 5.5 Reload stiffness, k (kip/in.) versus displacement, *w* (in.) for tests in silty sand

5.3.4 Summary of Reload Stiffness versus Displacement

Figure 5.6 shows the measured reload stiffness versus displacement for all tests. Different symbols are used to display the data from different soil configurations. In general, the measured reload stiffness is initially large before decreasing toward a constant value as displacement increases. Some scatter exists, but in general data from tests in all soil configurations reaches a constant value with displacement.

Initially, the reload stiffness was large in tests with clean sand. As displacement increased the reload stiffness reached a constant value. In tests with dense sand, the magnitude of displacement observed was lower than in tests with loose sand. The general trend observed showed that the reload stiffness in dense sand was likely decreasing toward the same value observed in loose sand tests at similar displacements.

In tests with the silty sand the reload stiffness remained constant with some scatter as displacement increased. The values for reload stiffness at large displacements in silty sand are similar to the values observed in the clean sand tests.

In general, the overburden stress applied during testing did not show a significant impact on the reload stiffness. Results from tests with high overburden pressures were mixed in with tests with low overburden pressures.

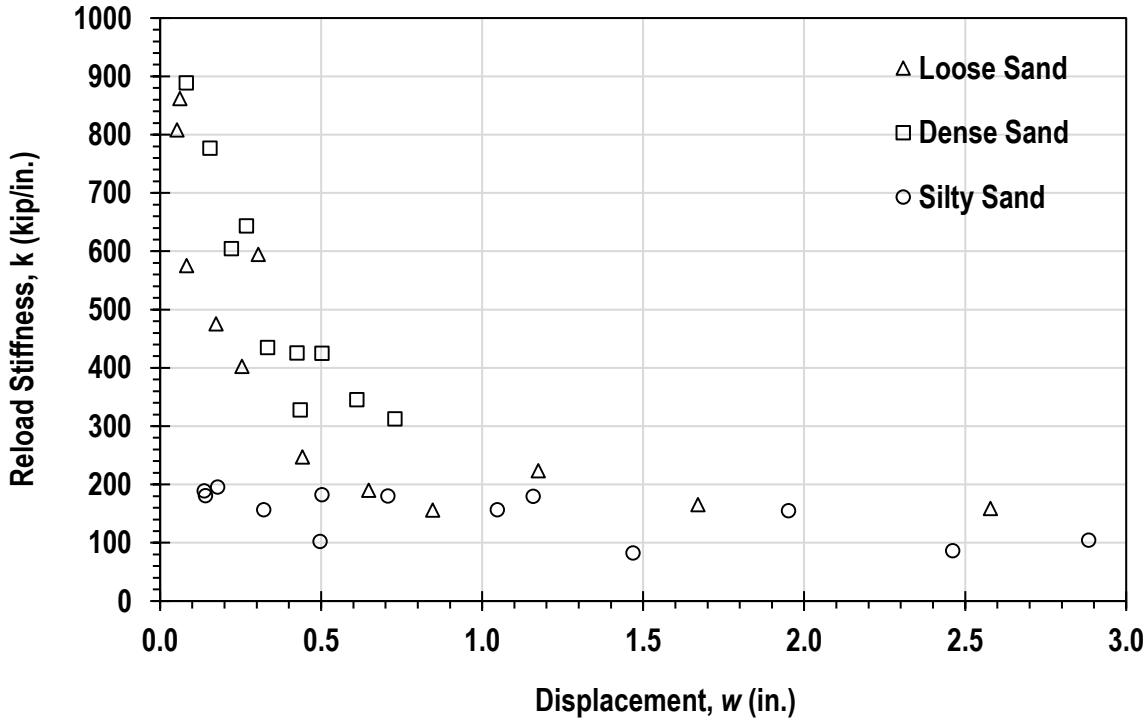

Figure 5.6 Reload stiffness, k (kip/in.) versus displacement, *w* (in.) for all tests

5.4 Normalized Reload Stiffness

It was noted after successive load-unload-reload cycles that the reload soil stiffness reached a constant value after undergoing significant displacement. In each soil configuration the reload soil stiffness was normalized by a reference stiffness. The reference stiffness was shown for each soil configuration was based on an exponential fit for loose sand and dense sand. The

trend in the data showed the reload stiffness reaching a constant value at large displacements. This constant value provided an ideal value to normalize the clean sand tests to.

In silty sand, the reload stiffness remained constant as displacement increased with some scatter. A linear line was fit to this data and used as a reference stiffness to normalize by. The values for the reference stiffness used are detailed by soil configuration in Table 5.1.

Table 5.1 Summary of reference stiffness values used by soil configuration for all tests

Soil Type	**Reference Stiffness (kip/in.)**
Loose Sand	172
Dense Sand	362
Silty Sand	128

Figure 5.7 is a plot of the normalized reload stiffness versus displacement for all tests. The data follows a similar trend observed in Figure 5.6. The normalized reload stiffness is initially large before decreasing toward a constant value as displacement increases. The data in the normalized reload stiffness versus displacement exhibits far less scatter. This suggests that using a reference stiffness to normalize the data is reasonable.

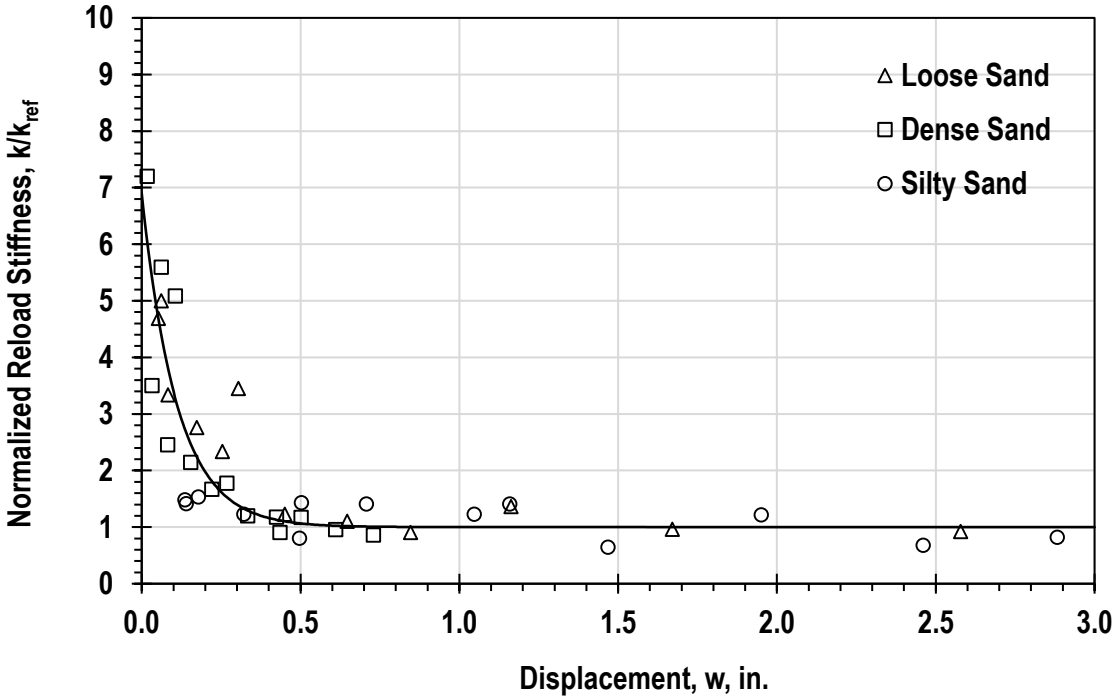

Figure 5.7 Normalized reload stiffness, k/k_{ref} versus displacement, *w* (in.) for all tests

In order to represent the trend examined in this work a relationship between normalized soil stiffness and displacement was developed. Equation 1 shows the relationship between reload stiffness (*k*), reference stiffness (k_{ref}), displacement (*w*) and the exponential function (*e*).

$$k / k_{ref} = 5.9e^{-9w} + 1 \qquad \text{(eq. 5.1)}$$

5.5 Comparison to values observed in literature

Gavin and Lehane (2007) performed a field load test on a physical model drilled shaft foundation to examine the factors controlling the base pressure versus settlement response under static loading. Figure 5.7 is a plot of the base force versus displacement from the test. The field

load tests were performed in an excavated area 20m below original ground surface in heavily overconsolidated glacially overridden sand. The overconsolidation ratio was 50 +/- 15 with an estimated preconsolidation stress near 29200 psf. The sand was fine with mean effective particle size (D_{50}) of 0.12 +/- 0.03 mm and a water content between 10 and 12 percent.

The axial load-displacement data from Gavin and Lehane (2007) was analyzed identical to the analysis procedure described in Section 5.1. The results of the analysis of this data are shown in Table 5.2. A total of four reload stiffnesses were taken from the plot and compared to the existing data from this testing program.

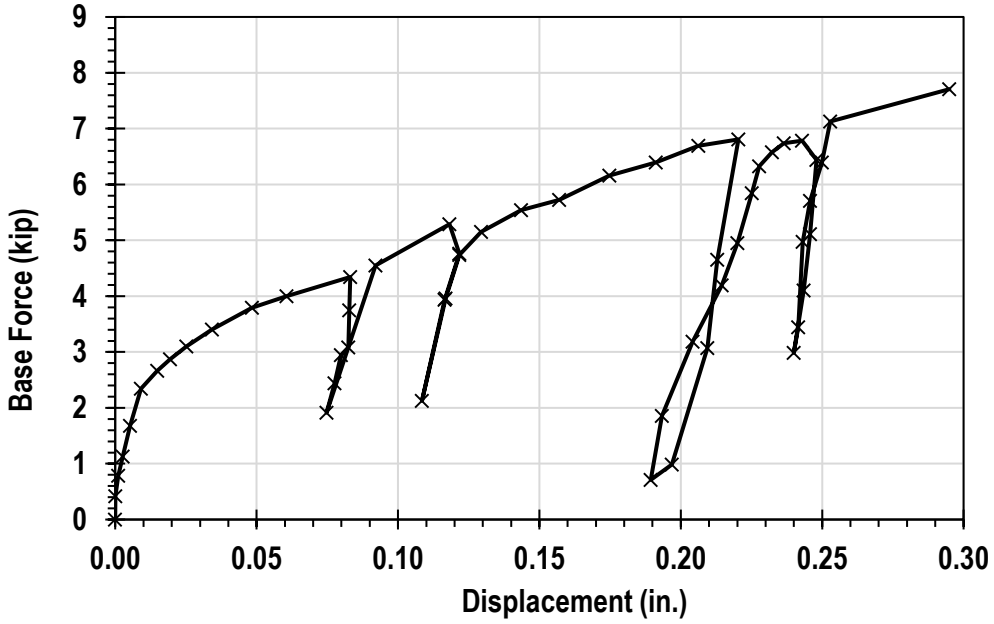

Figure 5.8 Base force versus displacement for model drilled shaft foundation from Gavin and Lehane (2007)

Table 5.2 Reload stiffness (kip/in.), displacement (in.) for each reloading cycle observed in Gavin and Lehane (2007) load tests on model drilled shaft foundation

Reloading Cycle	Reload Stiffness (kip/in.)	Displacement (in.)
1	151.2	0.092
2	200.0	0.121
3	146.4	0.228
4	319.2	0.253

Figure 5.8 is a plot of the reload stiffness values for loose sand, dense sand and silty sand calculated in this testing program versus the values taken from Gavin and Lehane (2007). Overall, the values observed in Gavin and Lehane (2007) compare well with the values observed in this testing program.

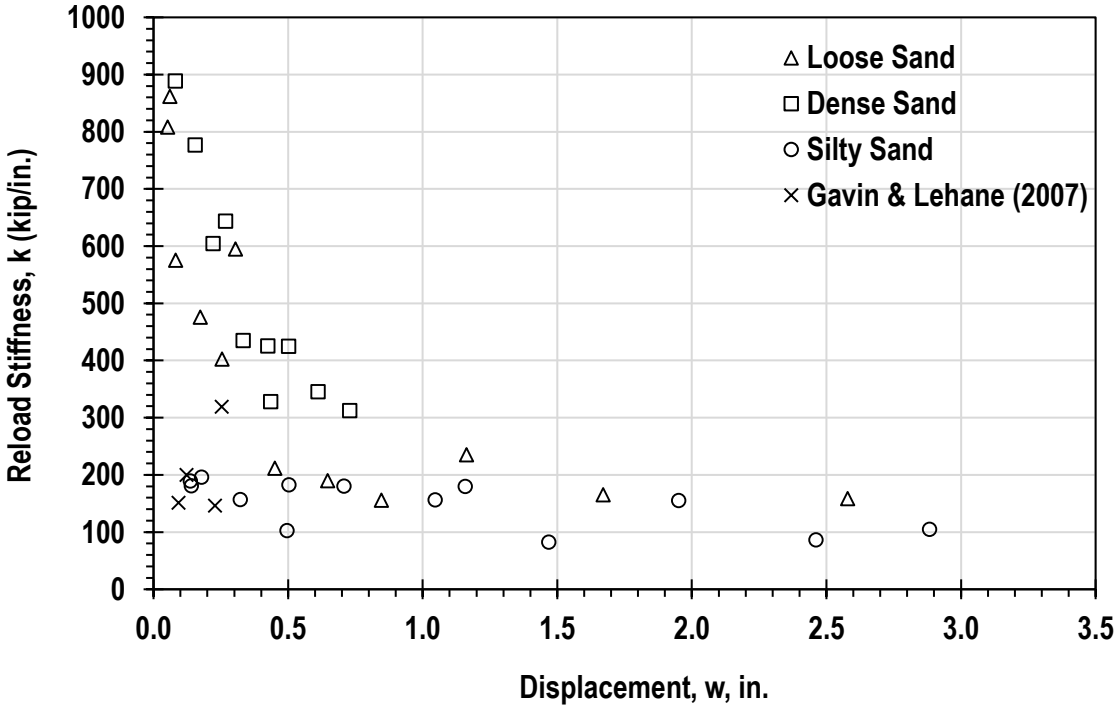

Figure 5.9 Reload stiffness, k (kip/in.) versus displacement, w (in.) showing results from this testing program and Gavin and Lehane (2007)

5.6 Summary

This chapter presented an analysis of nine axial load tests performed on model drilled shaft foundations. The load tests were performed in three different soil configurations in an experimental apparatus. The model foundation was subject to mulitple load-unload cycles where a reload stiffness could be determined. An analysis was performed to fit linear lines to the reload portion of the axial load-displacement results. The reload soil stiffness was plotted versus displacement based on soil configuration. A review of observed reload stiffnesses with model drilled shaft foundations in coarse grained soils was performed. The results from this testing program were reasonable compared to the results from Gavin and Lehane (2007).

A relationship between reload stiffness and displacement was created. In general, the reload stiffness is initially large at small displacements. As displacement increases the reload stiffness reaches a constant value in all soil configurations. The trend in the data observed in this testing program allowed for normalization. The constant portion of the plot of reload stiffness versus displacement allowed for a function to be fit to the data. A reference stiffness was taken from the exponential function and used to normalize the data. After normalizing the reload stiffness by a reference stiffness a relationship was developed. The relationship can be used to estimate the reload stiffness in model drilled shaft foundations in coarse grained soils.

Chapter 6 Summary, Conclusions and Recommendations

6.1 Summary

Drilled shaft foundations are a widely implemented type of deep foundation used to support large superstructures such as buildings, bridges and signage. Limitations exist in the full mobilization of the base resistance in drilled shaft foundations due to the nature of their installation method. A better understanding of the soil response at the base of drilled shaft foundations in coarse grained soils can lead to more accurate predictions of shaft response to loading. A laboratory testing program was developed and executed to determine the reload stiffness of a model drilled shaft in different soil configurations at varying magnitudes of displacement. Descriptions of the work performed to construct, instrument and test a model drilled shaft are presented in this thesis. Data from the testing program, and results from the analysis are also presented in this thesis.

In Chapter 2 an overview of drilled shaft foundations was provided. Relevant information regarding load transfer and base response of drilled shafts was also presented. Examinations of reload stiffness from literature were discussed. A procedure for a standard static axial load test from ASTM was summarized in this chapter.

Chapter 3 detailed the experimental apparatus used in this testing program. The apparatus includes a chamber assembly, reaction frame, bladder system, foundations, two different soils, and an instrumentation system to measure axial load, bladder pressure, strain from two different types of gages, vertical movement and soil density. Each component was described in detail. The testing procedure including assembly, testing and disassembly of the experimental apparatus was also explained.

Results of the testing program were presented in Chapter 4. The results were detailed on a test-by-test basis and divided into sections based on soil configuration. Relevant information about specific testing conditions are presented in each subsection. Results of the axial load-displacement tests are presented.

In Chapter 5 an analysis of nine axial load tests performed on model drilled shaft foundations was performed. The load tests were performed in three different soil configurations in an experimental apparatus. The model foundation was subject to mulitple load-unload cycles where a reload stiffness could be determined. The reload soil stiffness was plotted versus displacement based on soil configuration. A review of observed reload stiffnesses with model drilled shaft foundations in coarse grained soils was performed. The results from this testing program were reasonable compared to the results from Gavin and Lehane (2007).

A relationship between reload stiffness and displacement was created. In general, the reload stiffness is initially large at small displacements. As displacement increases the reload stiffness reaches a constant value in all soil configurations. The trend in the data observed in this testing program allowed for normalization. The constant portion of the plot of reload stiffness versus displacement allowed for a function to be fit to the data. A reference stiffness was taken from the exponential function and used to normalize the data. After normalizing the reload stiffness by a reference stiffness a relationship was developed. The relationship can be used to estimate the reload stiffness in model drilled shaft foundations in coarse grained soils.

A brief summary of the work performed in this testing program is described in this chapter. Conclusions from the data analysis specifically relating to the reload stiffness of model drilled shafts are presented. Finally, recommendations for further research are suggested.

6.2 Conclusions

The results of this testing program provided several conclusions regarding model drilled shaft foundations in coarse grained soils. Specifically, the reload stiffness determined during axial load-displacement tests was examined. Conclusions regarding the experimental apparatus as a means for testing model drilled shaft foundations were also drawn.

The reload stiffness after subsequent loading-unloading-reloading cycles changed as the overall displacement of the model foundation increased. In tests with loose poorly graded clean sand the reload stiffness was initially large at small displacements. As displacement increased the reload stiffness reached a constant value. Tests in dense poorly graded clean sand exhibited similar behavior to tests in the loose configuration. Initially at small displacements the reload stiffness was large before decreasing as displacement increased. The magnitude of the reload stiffness at similar displacements was larger in dense sand compared to loose sand.

In tests with compacted silty sand, the reload stiffness remained constant as displacement increased. In these tests the overall change in the reload stiffness was very small and was negligible when considering the scatter observed. The magnitude of the reload stiffness at large displacements was less than both dense and loose clean sand.

It was noted across all soil configurations that the overburden stress applied by the bladder system did not have a significant impact on the reload stiffness. Soil configuration, specifically density, played the largest role in the magnitude of the reload stiffness versus displacement.

In tests with compacted silty sand the water content at placement played a large role in soil behavior. Compacting the soil 1-2% wet of the optimum water content determined using the Standard Proctor test was ideal for workability and strength.

The relationship developed between reload stiffness and displacement was ideal for normalization. When testing each soil configuration, the data showed the reload stiffness reaching a constant value at large displacement. After normalizing by a reference stiffness in this constant range the normalized reload stiffness versus displacement showed less scatter. The reduction in scatter proved that normalization was effective.

Gavin and Lehane (2007) performed axial load tests on a model drilled shaft foundation in coarse grained soil. Analysis of the axial load-displacement data showed that the reload stiffness observed in this testing program was similar to the reload stiffness for model drilled shaft foundations in the field. This confirmed that the data was within a reasonable expected range to values and the experimental apparatus provided a reasonable means for examining the load-deformation response of coarse grained soils.

6.3 Lessons Learned

The experimental apparatus used in this program proved to be an effective means for evaluating the response of drilled shaft foundations under axial load. The apparatus allowed for numerous axial load tests to be completed in a controlled environment where several variables could be held constant. The apparatus had key components similar to what would be used in a field load test including a reaction frame and hydraulic system. The apparatus also had the ability to evaluate the response of drilled shafts at various vertical effective stresses with the use of the bladder system. The instrumentation system employed in this testing also resembled

instrumentation used in field load tests. The system recorded consistent, detailed and reliable results of axial load, vertical displacement, air pressure and axial strain. Having a program to record these variables was vital in the data reduction phase over hand measurements.

Additionally, the following topics were noted throughout the testing program as important lessons learned.

- A calibration chamber provides a reasonable and repeatable method for evaluating the response of drilled shaft foundations to axial load in coarse grained soils.
- Excavation of soil from the chamber is best done manually. Although laborious, excavation with a soil vacuum or large machinery such as a loader is inefficient.
- Compaction by hand with a soil tamper is more reliable and repeatable than compaction with any motorized machinery given the size and constraints of working in an experimental apparatus similar to what was used in this work.
- Having a hydraulic pump with a bypass valve is important to any work that requires a pressure (load) to be held with any reliability.
- Use of electronic instrumentation that can be recorded with computer software is extremely useful. Software such as LabVIEW allows for accurate measurements up to one data point per second and permits for multiple devices to be read at one time.

6.4 Recommendations

Throughout the testing program several recommendations were noted for future work pertaining to the testing of model drilled shaft foundations in cohesionless soils.

- Application of the relationship developed for model drilled shaft foundations to full size drilled shaft foundations. An examination of preexisting load test data can be

used to compare the reload stiffness observed in model tests to field load tests. Comparison of the results can lead to a broader use of the relationship with model and full size drilled shaft foundations in the field.

- Examination of the base load response of drilled shafts in coarse grained soils under axial load has shown that the stiffness degradation of the shaft can vary greatly based on the overconsolidation ratio of the soil (Gavin and Lehane, 2007). Specifically, the reload stiffness degrades at smaller strains in soils with low overconsolidation ratios compared to coarse grained soils with high overconsolidation ratios. Undertaking a study to evaluate the factor overconsolidation ratio can have on the reload stiffness would be valuable.
- Performing axial load-displacement tests on large scale physical model drilled shaft foundations with a grout delivery system. Post-grouting the models could provide a comparison to the ungrouted shafts examined in this thesis.
- Use of a smaller diameter model foundation could eliminate possibly interaction with the experimental apparatus during testing. Thiyyakkandi et al. (2014) noted during their testing of model drilled shaft foundations in a similar experimental apparatus that the lateral boundary of the chamber may influence the stress and displacement field near the foundation. They report that the radial zone of influence to be in the range of 3 to 8 pile diameters.

REFERENCES

American Society for Testing and Material, ASTM (2017). Annual Book of Standards, ASTM D1143, Standard Test Methods for Deep Foundations Under Static Axial Compressive Load.

American Society for Testing and Material, ASTM (2017). Annual Book of Standards, ASTM D2216, Standard Test Methods for Laboratory Determination of Water (Moisture) Content of Soil and Rock by Mass.

American Society for Testing and Material, ASTM (2017). Annual Book of Standards, ASTM D2487, Standard Practice for Classification of Soils for Engineering Purposes (Unified Soil Classification System).

American Society for Testing and Material, ASTM (2017). Annual Book of Standards, ASTM D4253, Standard Test Methods for Maximum Index Density and Unit Weight of Soils Using a Vibratory Table.

American Society for Testing and Material, ASTM (2017). Annual Book of Standards, ASTM D4254, Standard Test Methods for Minimum Index Density and Unit Weight of Soils and Calculation of Relative Density.

American Society for Testing and Material, ASTM (2017). Annual Book of Standards, ASTM D6528, Standard Test Method for Consolidated Undrained Direct Simple Shear Testing of Fine Grain Soils.

American Society for Testing and Material, ASTM (2017). Annual Book of Standards, ASTM D6913, Standard Test Methods for Particle-Size Distribution (Gradation) of Soils Using Sieve Analysis.

Coduto, D.P., Kitch W.A and Yeung, M.R. (2016). Foundation Design Principles and Practices, 3rd Ed, Pearson Education, Upper Saddle River, NJ.

Dias, T. and Bezuijen, A. (2017). "Load-Transfer Method for Piles under Axial loading and Unloading." *Journal of Geotechnical and Geoenvironmental Engineering,* 144(1), 1-9. DOI 10.1061/(ASCE)GT.1943-5606.0001808

Gavin, K. and Lehane B. (2007). "Base Load – Displacement Response of Piles in Sand." *Canadian Geotechnical Journal,* 44, 1053-1062. DOI 10.1139/T07-048

Loehr et al. (2016). "State of the Practice of Post-grouting of Drilled Shaft Foundations.", 1-7

Reese, L. and O'Neil, M. (1999). "Drilled Shafts: Construction Procedures and Design Methods.", 290-293.

Thiyyakkandi et al. (2014). "Experimental Study, Numerical Modeling of and Axial Prediction Approach to Base Grouted Drilled Shafts in Cohesionless Soils." *Acta Geotechnica,* 9, 439-454. DOI 10.1007/s11440-013-0246-3

APPENDIX A: TABULATED DATA

Test No.	Average Overburden Stress (psi)	Reload Stiffness (kip/in.)	Base Force (kip)	Base Stress (kip/ft^2)	Beginning Displacement (in.)	Final Displacement (in.)	Normalized Stiffness (k/kref)
1	10.1	575.33	5.178	3.699	0.073	0.082	3.34
1	10.1	475.62	10.290	7.350	0.152	0.173	2.76
1	10.1	211.96	16.859	12.042	0.372	0.450	1.23
1	10.1	235.45	25.548	18.249	1.054	1.162	1.37
2	20.5	808.13	6.542	4.673	0.044	0.052	4.69
2	20.5	402.59	16.553	11.824	0.213	0.254	2.34
2	20.5	190.05	25.123	17.945	0.515	0.647	1.10
2	20.5	165.37	33.966	24.261	1.465	1.670	0.96
2	20.5	158.84	39.446	28.176	2.330	2.578	0.92
3	30.2	861.99	3.013	2.152	0.057	0.061	5.00
3	30.2	594.73	11.535	8.240	0.286	0.304	3.45
3	30.2	155.98	21.351	15.251	0.709	0.846	0.90
4	10.4	328.27	34.138	24.384	0.331	0.435	0.91
4	10.4	345.56	50.887	36.348	0.464	0.611	0.95
5	20.5	1269.8	7.070	5.050	0.027	0.032	3.50
5	20.5	888.7	12.864	9.189	0.066	0.081	2.45
5	20.5	777.04	19.898	14.213	0.128	0.154	2.14
5	20.5	643.64	32.845	23.461	0.218	0.267	1.78
5	20.5	425.09	51.865	37.047	0.380	0.502	1.17
5	20.5	312.62	68.845	49.175	0.509	0.729	0.86
6	30.2	2608.8	3.422	2.444	0.015	0.017	7.20
6	30.2	2027.9	12.188	8.706	0.056	0.062	5.60
6	30.2	1842.5	20.023	14.302	0.095	0.105	5.08
6	30.2	604.76	35.828	25.592	0.161	0.220	1.67
6	30.2	435.22	48.093	34.352	0.223	0.333	1.20
6	30.2	425.54	59.801	42.715	0.284	0.424	1.17
7	10.3	180.69	3.505	2.504	0.120	0.140	1.41
7	10.3	102.55	6.643	4.745	0.431	0.496	0.80
7	10.3	82.678	9.851	7.037	1.348	1.468	0.65
7	10.3	86.415	12.550	8.964	2.315	2.461	0.68
8	18.8	195.77	3.303	2.360	0.160	0.178	1.53
8	18.8	182.44	6.049	4.321	0.469	0.502	1.43
8	18.8	156.54	9.163	6.545	0.988	1.046	1.23
8	18.8	155.16	12.117	8.655	1.872	1.950	1.22

8	18.8	104.8	14.993	10.709	2.739	2.883	0.82
9	30.6	189.25	3.315	2.368	0.118	0.136	1.48
9	30.6	157	6.085	4.346	0.283	0.322	1.23
9	30.6	180.23	9.258	6.613	0.656	0.707	1.41
9	30.6	179.58	12.182	8.701	1.090	1.158	1.41